Géochronologie

Monazite de Trimouns.

Succession d'événements métasomatiques permiens et mésozoïques dans l'est des Pyrénées avec application sur le gisement de talc-chlorite de Trimouns

Résumé de l'article (Boutin et al., 2016)

Comme évoqué dans l'introduction, plusieurs études récentes renouvellent le modèle pré-orogénique des phases pré-alpines à alpines des Pyrénées. Ces travaux traitent notamment de l'amincissement crustal associé à l'exhumation tectonique du manteau dans la ***ZNP*** (Lagabrielle et Bodinier, 2008 ; Jammes et al., 2009 ; Lagabrielle et al., 2010 ; Clerc, 2012 ; Clerc et al., 2012 ; Corre et al., 2016 ; Saint Blanquat et al., 2016). Des questions demeurent sur la formation de ce domaine hyper étendu, et sur la période précise d'exhumation du manteau par cassure de la croûte lithosphérique.

Il y a une quinzaine d'années, une étude géochronologique majeure (Schärer et al., 1999) a démontré que la minéralisation de Trimouns était ancrée dans le cycle orogénique alpin (pré-collision - ca. 100 Ma) alors que celle-ci était jusqu'alors considérée comme hercynienne. Cette étude permit d'apporter des éléments de réponse aux questions relatives aux Pyrénées alpines. Elle met en relation les terrains paléozoïques de Trimouns et l'amincissement crustal (Boulvais et al., 2006). Elle permet d'inscrire l'hydrothermalisme « talqueux » dans la période de rifting pyrénéen (Crétacé « moyen »), et par conséquent dans une période contemporaine de l'exhumation mantellique des modèles cités précédemment.

Cependant, la discussion autour de « l'âge de Trimouns » n'est pas close, et l'étude de Schärer et al. (1999) mérite un approfondissement pour deux raisons. La première est que talc et chlorite ne pouvant pas (encore) être « directement » les objets de datations. Pour dater le gisement, Schärer & al. (1999) utilisent deux minéraux de terres rares contemporains de la talcification : xénotime et monazite. Or ces minéraux se limitent à une zone bien précise du gisement, la zone des minéraux à terres rares dans les dolomies du toit (secteur P2 - **Fig. IV-1** et **Fig. I-32**). Cette zone est bien trop localisée pour représenter un gisement hétérogène. La seconde raison est, que depuis une quinzaine d'années, les techniques de datation ont évolué et plusieurs autres espèces minérales comme les titanites se sont révélées être de bons marqueurs géochronologiques (Frost et al., 2000).

L'étude présentée ici (Boutin et al., 2016) prolonge donc les travaux de Schärer et al. (1999) avec le souci d'appliquer des techniques de datation éprouvées sur un plus large panel de minéraux répartis sur les différentes formations du site. Dans cette optique nous avons réalisé un échantillonnage plus fin des minéraux associés aux différents terrains sur Trimouns. L'étude géochronologique U-Th-Pb a été menée à l'ICP-MS à ablation laser sur des minéraux de terres rares (xénotime, monazite, allanite), et sur des

minéraux titanifères (titanite, rutile). En parallèle à Trimouns, nous avons pu effectuer des travaux similaires sur des gisements de talc-chlorite de la ***ZA*** : le gisement de Caillau au col de Jau, et le gisement de Las Embollas (**Fig. IV-1**). Ces sites sont plus éloignés du domaine hyper-étendu crétacé et permettent une mise en perspective des âges obtenus sur les minéralisations talco-chloriteuse en fonction du contexte géologique.

Sur Trimouns, l'ensemble des données montre que le gisement a été formé pendant au moins deux événements hydrothermaux successifs.

1) Le premier a été révélé par des titanites contenues dans les chloritites. Il est principalement relié à une partie de la veine chloriteuse (proche du mur). Cet évènement est estimé autour de 165 Ma (Jurassique moyen), et est probablement lié à l'événement hydrothermal jurassique décrit par Cathelineau et al. (2012) à l'échelle de l'Europe occidentale (**Fig. IV-1**).
2) Le second événement a duré entre 25 et 30 millions d'années (entre ca. 122 Ma et 96 Ma, entre la fin de l'Aptien et Cénomanien). Avec les résultats obtenus, cet épisode peut être découpé en trois sous-événements interprétés comme des « pulses » de circulation hydrothermale. Ce métasomatisme est révélé par des minéraux de terres rares et titanifères ce qui permet de le relier à la fois aux formations de talcitites et des chloritites. Cet événement est l'expression géologique de l'amincissement de la croûte terrestre résultant de l'ouverture du golfe de Gascogne.

Au Jurassique, la formation de chloritites induit une zone de forte perméabilité et de faiblesse mécanique le long de laquelle les déformations et les circulations de fluides ont pu être favorisées lors du second événement au Crétacé.

Les autres gisements de la zone axiale (col de Jau et de Las Embollas) présentent des minéralisations d'âges différents.

Au col de Jau, deux événements hydrothermaux sont relevés dans des chloritites ; un événement permien à ca. 296 Ma associé à la fin du Varisque, et un second entre le Crétacé et le Jurassique à 141 Ma (+/- 8 Ma) durant le début du rifting Pyrénéen.

A Las Embollas, les talcitites semblent être marquées par un seul évènement hydrothermal permien à ca. 270 Ma (fini-varisque).

Dans les Pyrénées, l'histoire des circulations hydrothermales formant les minerais talco-chloriteux a pu être décrite avec ces trois gisements.

On observe une succession complexe d'événements :

1) à la fin du Varisque, un événement de chloritisation dans la ***ZA*** probablement lié à la fin du magmatisme et aux déformations varisques ;
2) au Permien, un événement de formation de talc dans la ***ZA*** ; il est potentiellement lié à l'extension tardi-varisque qui sépare les cycles hercynien et alpin ;
3) des événements jurassiques liés à la formation de chlorites (voir de talc) et associés aux prémices du rifting décrit en Europe occidentale (Cathelineau et al., 2012) ;
4) un événement majeur de formation de talc et de chlorites au Crétacé ; il pourrait être le résultat d'une activité axée autour de trois « pulses » hydrothermaux.

Ce dernier événement est spatialement et temporellement associé aux métasomatismes sodique et calco-sodique (Boulvais et al., 2007 ; Poujol et al., 2010 ; Fallourd et al., 2014) observés dans la région (**Fig. IV-1**), ou à l'Ouest de la chaîne (Corre et al., 2016). Tous ces événements hydrothermaux sont corrélables à des tectoniques extensives (Cathelineau et al., 2012).

Nos données confirment que le métasomatisme a commencé avant le métamorphisme nord pyrénéen (et avant le magmatisme associé), (**Fig. IV-1**). L'évènement hydrothermal est considéré comme étant de basse à moyenne température (250°C à 350°C - Parseval, 1992 ; Boiron et al., 2005) ; à l'inverse le métamorphisme nord pyrénéen présente des températures élevées (maximum entre 500°C et 600°C - Golberg et Leyreloup, 1990). Le décalage temporel entre basse et forte température suggère un changement de configuration géodynamique entre ces deux périodes. L'exhumation du manteau (source de chaleur) a pu être initiée entre la période « froide » marquée par l'évènement crétacé de Trimouns, et la période « chaude » du métamorphisme nord pyrénéen (Cénomano-Turonien).

D'un point de vue méthodologique, notre étude confirme la robustesse de la titanite. En effet, ces minéraux titanifères étudiés donnent des âges permiens et jurassiques or ils ont connu/subi deux événements hydrothermaux avérés (permien et jurassique au Col de Jau - jurassique et crétacé à Trimouns). Ayant conservé l'empreinte de l'événement le plus ancien, ils n'ont donc pas été perturbés ou « remis à zéro » (formule consacrée des géochronologues) par les circulations de fluides de moyenne température (id 300°C) qui ont suivi.

N.B. : les données brutes contenues de l'article (« Electronic supplementary material ») sont fournies en **annexe 5**.

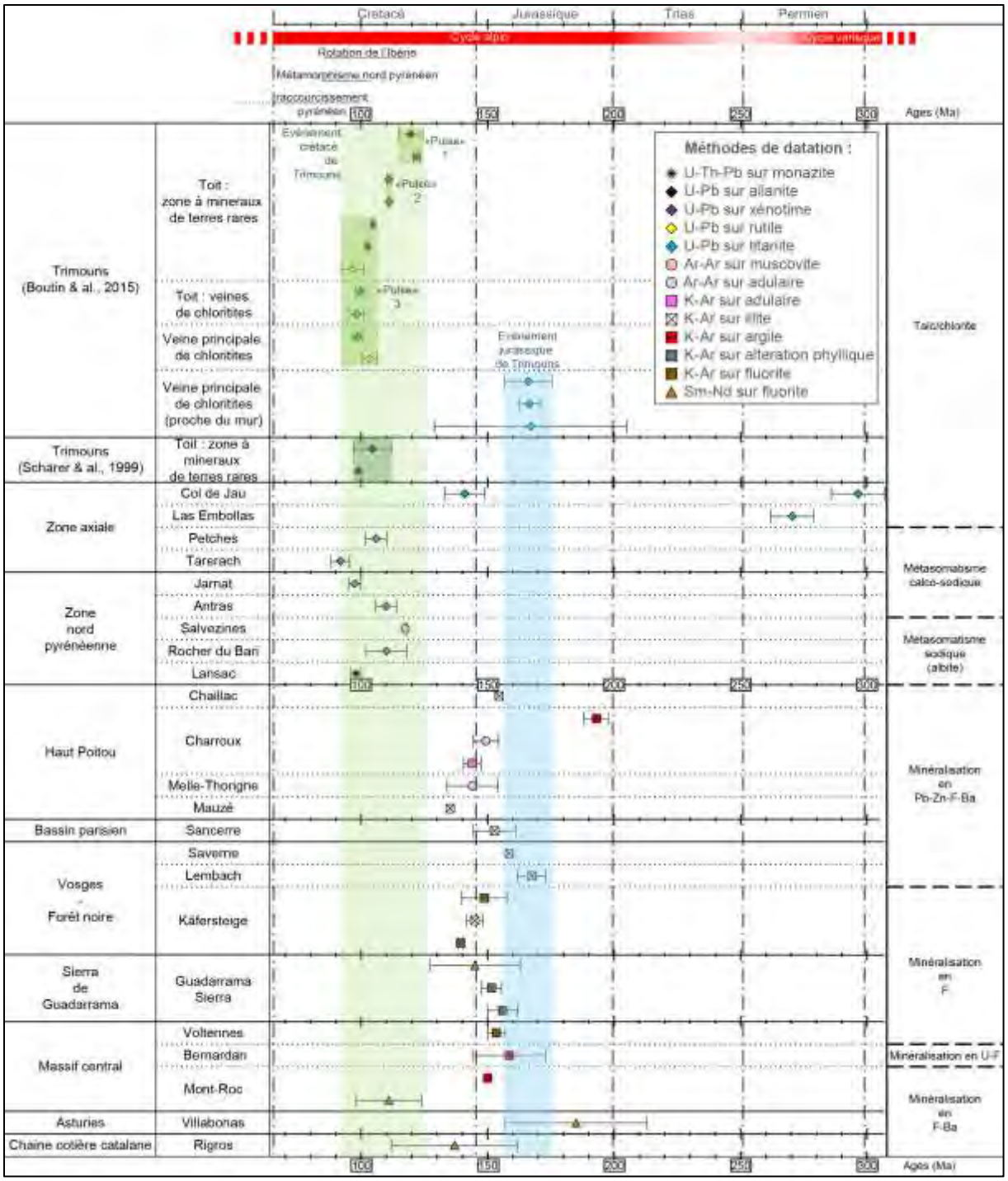

Figure IV-1 : Chronologie des datations à la carrière de Trimouns et des minéralisations en Europe occidentale. *Modifiée de Boutin & al. (2015).*

Les pages suivantes présentent l'article tel qu'il est publié dans la revue « International Journal of Earth Sciences ».

Int J Earth Sci (Geol Rundsch) (2016) 105:747–770
DOI 10.1007/s00531-015-1223-x

ORIGINAL PAPER

Succession of Permian and Mesozoic metasomatic events in the eastern Pyrenees with emphasis on the Trimouns talc–chlorite deposit

Alexandre Boutin[1,2] · Michel de Saint Blanquat[1] · Marc Poujol[3] · Philippe Boulvais[3] · Philippe de Parseval[1] · Caroline Rouleau[3] · Jean-François Robert[4]

Received: 13 February 2015 / Accepted: 20 June 2015 / Published online: 15 July 2015

Abstract Recent studies proposing pre-orogenic mantle exhumation models have helped renew the interest of the geosciences community in the Pyrenees, which should be now interpreted as a hyper-extended passive margin before the convergence between Iberia and Eurasia occurred. Unresolved questions of the Pyrenean geology, as well as the understanding of the formation of hyper-extended passive margins, are how the crust was thinned, and when, where and how the crustal breakoff occurred. The study of the Variscan and pre-Variscan Pyrenean basement is thus critical to document and understand this Cretaceous crustal thinning. In order to specify the timing of Mesozoic metasomatism and the associated deformation in the pre-Mesozoic basement of the Pyrenees, we carried out a U–Th–Pb laser ablation ICP–MS study on a large panel of REE and titanium-rich minerals (titanite and rutile) from talc–chlorite ores from the eastern Pyrenees, with a special emphasis on the Trimouns deposit, the world's largest talc quarry. Our results suggest that the Trimouns talc formation was restricted to the upper Aptian–Cenomanian time, while the talc and chlorite formation in the eastern Pyrenees occurred during several distinct Permian, Jurassic and Cretaceous episodes. These results give strong constraints on the tectonic setting of the Pyrenean domain during the transition between the Variscan and Alpine orogenic cycles, and particularly on when and how the upper crust was thinned before the crustal breakoff and the final mantle exhumation.

Keywords Trimouns · Talc · Chlorite · Pyrenees · Rifting · Metasomatism · LA–ICP–MS U–Th–Pb dating

Introduction

Geological studies of the Pyrenees have generated, and continue to generate, numerous controversies due to its highly debated plate kinematic framework (Le Pichon et al. 1970; Choukroune and Mattauer 1978; Olivet 1996; Sibuet et al. 2004; Gong et al. 2008; Bronner et al. 2011; Tucholke and Sibuet 2012; Bronner et al. 2012) and complex geological and geophysical characteristics (Barnolas and Chiron 1995; Chevrot et al. 2014). Recent models proposing pre-orogenic mantle exhumation have helped renew the interest of the geosciences community in this orogen. Recent data have shown that the outcropping conditions of mantle rocks exposed in the Pyrenees imply the fragmentation of the mantle at or near the surface and its mixing with the already deformed and metamorphosed Mesozoic cover (Lagabrielle and Bodinier 2008). This implies that the Pyrenean domain underwent a major phase of exhumation of the subcontinental mantle during the mid-Cretaceous (Lagabrielle and Bodinier 2008; Jammes et al. 2009; Lagabrielle et al. 2010; Clerc et al. 2012). One of the major consequences is that the pre-orogenic Pyrenees should now be

Electronic supplementary material The online version of this article (doi:10.1007/s00531-015-1223-x) contains supplementary material, which is available to authorized users.

✉ Alexandre Boutin
alexandre.boutin@get.omp.eu

[1] Géosciences Environnement Toulouse, UMR 5563, Université de Toulouse, CNRS, IRD, 14 Avenue Edouard Belin, 31400 Toulouse Cedex 1, France

[2] Imerys Talc Luzenac France, 21 Rue Principale, 09250 Luzenac, France

[3] Géosciences Rennes, UMR 6118, Université Rennes 1, 35042 Rennes Cedex, France

[4] Imerys Talc Europe, 2 Place Edouard Bouillères, BP 33662, 31036 Toulouse Cedex 1, France

interpreted as a hyper-extended passive margin and that the internal north Pyrenean zone, which contains lherzolites, is a fossil analog of a distal passive margin where the thermomechanical processes of mantle exhumation and associated crustal thinning can be studied at the surface on exposed rocks (Masini et al. 2014; Clerc and Lagabrielle 2014). The main unresolved questions of the pre-orogenic Pyrenean geology, as well as the study of hyper-extended passive margins, are how the crust was thinned, and when, where and how the crustal breakoff occurred. The study of the Variscan and pre-Variscan basement is thus critical to documenting and understanding the Cretaceous crustal thinning.

In addition to the presence of lherzolites, another geological peculiarity of the Pyrenees can be observed in the basement and is represented by numerous occurrences of albitite (Pin et al. 2001, 2006; Monchoux et al. 2006; Boulvais et al. 2007; Poujol et al. 2010; Fallourd et al. 2014), chlorite and talc deposits (Aranitis 1967; Fortuné 1971). Because they are exposed within the Variscan massifs and were formed at the expense of Paleozoic or even older rocks, they were first interpreted as resulting from (late) Variscan events (Fortuné et al. 1980). However, recent geochronological and geochemical works have shown that the eastern Pyrenean albitites and the Trimouns talc deposits are in fact the products of one (or more) Mesozoic regional-scale hydrothermal event(s) (Schärer et al. 1999; Boulvais et al. 2006; Poujol et al. 2010; Fallourd et al. 2014). Consequently, the crustal thinning associated with the mantle exhumation and the formation of these deposits is contemporaneous and are both associated with intense fluid circulation and deformation of the pre-Alpine basement crustal rocks. These recent studies all emphasize the importance of fluids in the mechanical and chemical evolution of both mantellic and crustal rocks during crustal thinning and mantle exhumation and provide strong constraints on the syn-rift evolution of passive margins.

Located in the north Pyrenean Saint Barthelemy Massif (de Saint Blanquat 1989), the Trimouns talc deposit is exceptional because of its ore quality and quantity, as it is the world's largest active talc–chlorite quarry (Höffler and Vinandy 2000). A preliminary U–Pb geochronogical study on xenotime and monazite sampled in centimeter scale geodes from the hanging wall seems to demonstrate a continuous crystallization of these minerals between 112 and 97 Ma, which suggests that the Trimouns deposit is the result of a long-lasting Cretaceous hydrothermal activity (Schärer et al. 1999). Three points prevent us from considering that we have complete knowledge of these Cretaceous metasomatic events. First, the minerals from the Trimouns deposit dated by Schärer et al. (1999) were not spatially associated with the main ore body; second the complexity of the deposit, which is comprised of juxtaposed lenses of talc and chlorite ores that are not necessarily contemporaneous; and third, the occurrence of other non-dated talc and chlorite ores in the Pyrenees, mainly in the eastern part of the Axial Zone (Fortuné 1971).

The aim of this paper is therefore to provide more precise knowledge of the hydrothermal circulation(s) that occurred in the Pyrenean domain between the Variscan and Alpine orogenies. In order to do this and to be sure that we are dating the ore formation events themselves, we have selected titanium- and REE-rich minerals (titanite, rutile, monazite, xenotime and allanite) that were formed together with the talc and chlorite mineralization. Furthermore, in order to get a more regional picture, our study focuses on three different locations: Trimouns, where we worked on a larger area representative of the whole deposit, and two locations in the Pyrenean Axial Zone, Las Embollas (Corneilla de Conflent) and the Col de Jau (Caillau) ore deposits. Our results suggest a more complicated history for the Trimouns talc–chlorite formation than previously thought and give strong constraints on the tectonic setting of the Pyrenean domain during the transition between the Variscan and Alpine orogenic cycles, and particularly on the relationship between crustal extension and mantle exhumation in the Pyrenean rift.

Geological context

The Pyrenean mountain belt belongs to the Western European Alpine system and was constructed on the plate boundary which separates the Iberian and European plates. This plate boundary has been active since the Paleozoic, and therefore, the Pyrenees are an area where we can observe the superposition of two successive orogens on the same crustal segment; the Variscan orogeny at the end of the Paleozoic, and the Mesozoic–Cenozoic Alpine orogeny. Despite the fact that 200 Ma separates the youngest orogenic Variscan events from the oldest Alpine ones, these two orogens are difficult to differentiate on pre-Mesozoic rocks affected by both episodes. They share similar structural directions (EW to WNW-ESE), due to the reuse of Variscan structural discontinuities during the Alpine orogeny. In addition, they both have been marked by a strong HT-LP thermal event that, in both cases, reaches the amphibolite facies conditions (600 °C—Pin and Vielzeuf 1983; Vielzeuf 1984; de Saint Blanquat 1989; de Saint Blanquat 1993 for the Variscan orogeny—Golberg and Leyreloup 1990 for the Alpine orogeny). The Variscan orogeny in the Pyrenees is polyphased with a southwestward thrusting event followed by a dextral transpressive phase, accompanied by a large calc-alkaline magmatism and a HT-LP metamorphism (Debon et al. 1995; Denèle et al. 2014). The importance and characteristic of the late Variscan extensional event are still being discussed (de Saint Blanquat

et al. 1990). The Variscan Pyrenees were part of the external domain of the southwestern European Variscan orogeny. The Alpine Pyrenees are the result of the Cenozoic inversion of a Cretaceous transcurrent hyper-extended rift that was created during the opening of the Bay of Biscay (Le Pichon et al. 1970; Choukroune et al. 1973; Choukroune and Mattauer 1978; de Saint Blanquat et al. 1986; Olivet 1996; Lagabrielle and Bodinier 2008). Furthermore, a Miocene extensional phase, related to the rotation of the Corsica–Sardinia block and the opening of the Gulf of Lion, is present in the eastern part of the range.

The Pyrenees are characterized by a structural zonation parallel to the elongation of the belt (Fig. 1a). In our study area, we found (from north to south):

1. The north Pyrenean zone (NPZ) (Choukroune 1976), which thrusts the foreland Aquitaine basin toward the north via the north Pyrenean frontal thrust. It is made up of Mesozoic and Cenozoic sedimentary sequences, in particular the Albo-Cenomanian "Black-flysch" sequence (Debroas 1990), Triassic and Cretaceous magmatic rocks (Azambre and Rossy 1976; Béziat et al. 1991) and the so-called north Pyrenean massif (NPM) comprised of Paleozoic and upper Proterozoic metasedimentary and magmatic rocks that were mainly affected by Variscan or older events. The base of some massifs from the NPM (Agly, Bessède de Sault, St Barthelemy, Castillon and Ursuya) reached the granulite facies (Zwart 1954; Vielzeuf 1984; de Saint Blanquat et al. 1990; de Saint Blanquat 1993) ca. 300 Ma ago (Delaperrière et al. 1994). The southern part of the NPZ is comprised of the narrow "Internal Metamorphic Zone" (IMZ) which contains high-grade Mesozoic metasedimentary rocks (HT-LP metamorphism, 110-85 Ma: Albarède and Michard-Vitrac 1978; Golberg and Maluski 1988; Golberg and Leyreloup 1990), carbonate breccias enclosing lherzolite fragments (Lagabrielle and Bodinier 2008; Lagabrielle et al. 2010; Clerc et al. 2012) and catazonal Variscan granulitic slices. Recent works have shown that the IMZ corresponds to an area that experienced an extreme crustal thinning associated with the exhumation of the subcontinental mantle (Lagabrielle and Bodinier 2008; Lagabrielle et al. 2010; Clerc and Lagabrielle 2014).
2. The north Pyrenean fault (NPF) is the southern limit of the NPZ. Its importance, evolution and geometry have been the subject of major controversies. It is now recognized as representing one of the Cretaceous sinistral transform faults related to the opening of the Bay of Biscay. But it is older, since dextral movements ascribed to the end of the Variscan were described along this fault (Arthaud and Matte 1975; de Saint Blanquat 1993).
3. Located to the south of the NPF, the Axial Zone (AZ) consists of Paleozoic and upper Proterozoic metasedimentary series and magmatic rocks that primarily deformed during the Variscan orogeny, but also during the Alpine Cenozoic southward thrusting events (Séguret 1972; Choukroune et al. 1989; Muñoz 1992). It contains intrusive and effusive rocks of upper Pennsylvanian (ca. 305 Ma) to Permian age (ca. 267 Ma—Denèle et al. 2012), as well as rare fragments of Mesozoic sedimentary cover (Barnolas and Chiron 1995).

Talc–chlorite deposits are produced by the transformation of magnesian carbonates or ultramafic rocks. The deposits originating from ultramafic rocks and serpentinites were produced via alteration involving little chemical transfer since the chemical composition of the primary rocks is relatively similar to that of talc. No economic deposits are formed through the transformation of ultramafic rocks in the Pyrenees. The deposits originating from magnesian carbonates occur within the metasedimentary series where carbonate rocks are more or less abundant (dolomitic limestones, dolostones and magnesites); the talc originated from these carbonates. Chlorite ores are primarily composed of magnesian chlorite and were formed through the alteration of silico-aluminous rocks (micaschists, gneisses, granitic rocks, etc.). These deposits could be defined as metasomatic because there were significant chemical exchanges (high mobility of SiO_2, Mg, Na, K, Ca, CO_2, etc.) during their formation. They occur in zones of intense deformation, such as thrust and fracture zones, where hydrothermal circulation and thus fluid–rock exchange are significant (Moine et al. 1982a, b, 1989). Most of the Pyrenean talc and chlorite ores were formed by the metasomatism of carbonated and silico-aluminous rocks (Aranitis 1967; Fortuné 1971). The talc protolith is mainly comprised of lower Paleozoic marbles and dolostones. The chlorite protolith is comprised of gneisses, migmatites, micaschists and granitoids from the Variscan basement.

The Trimouns talc–chlorite deposit is located in the north Pyrenean Saint Barthelemy Massif (SBM). The SBM is made up of (Fig. 1b) (from bottom to top) (Zwart 1954; de Saint Blanquat 1989): (1) A paragneissic formation (2 km thick) probably derived from the upper Proterozoic series which have been metamorphosed during the late Variscan LP-HT granulitic facies, (2) migmatites and micaschists mainly derived from the lower Paleozoic series (2 km thick) and intruded by granodioritic and leucogranitic sills, (3) an upper Paleozoic series. During the late Cretaceous and Tertiary, the massif was unroofed and overthrust to the north along south dipping reverse faults. The contact between the gneiss and migmatite is a ductile fault, the so-called Main Mylonite Band (Passchier 1982; de Saint Blanquat et al. 1990; de Saint Blanquat 1993). The contact between the

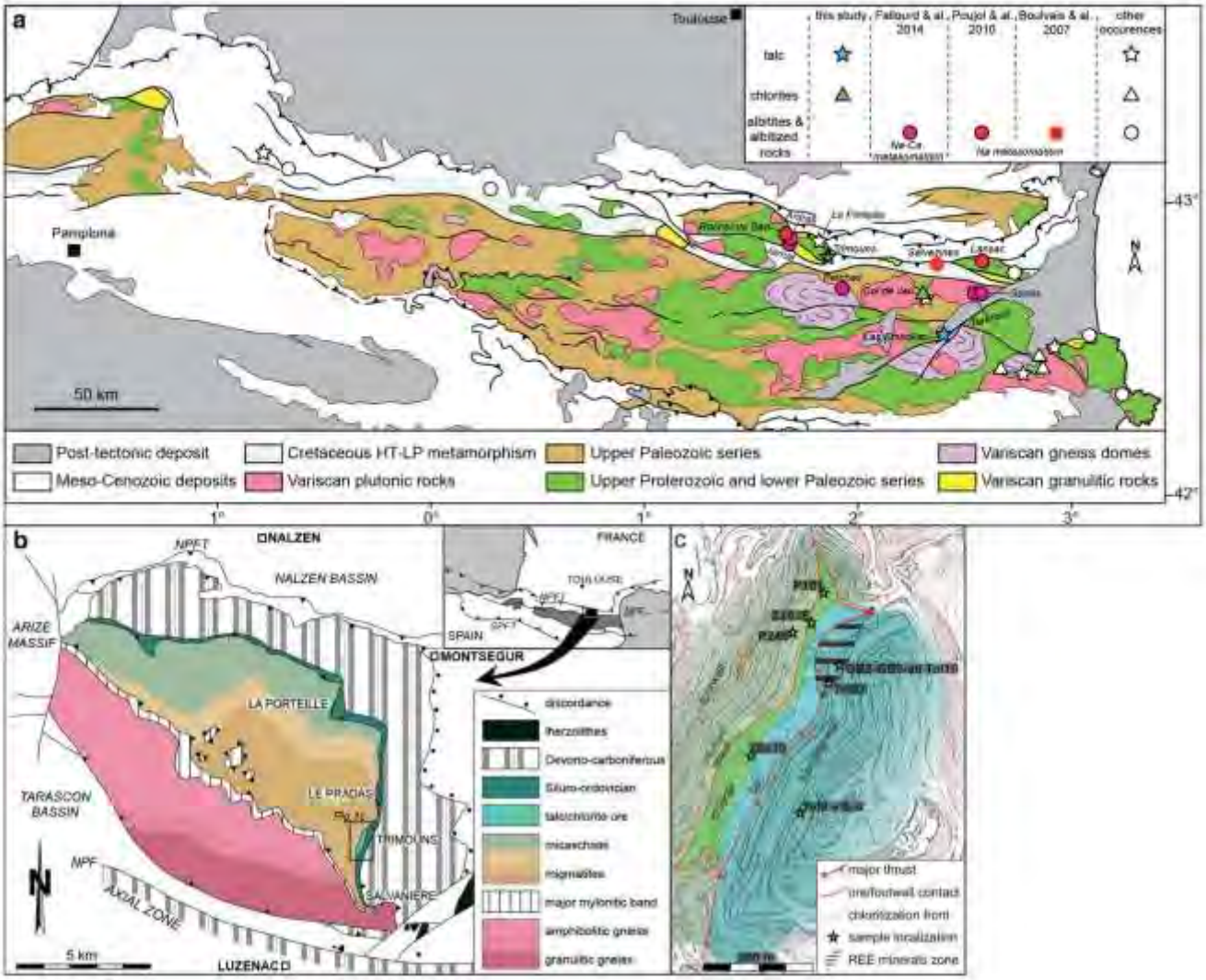

Fig. 1 **a** Simplified geological map of the Pyrenees with the location of the dated talc, chlorite and albitite mineralizations, **b** geological map of the Saint Barthelemy massif (from de Saint Blanquat 1989), **c** schematic map of the Trimouns ore with sample locations

lower Paleozoic micaschists and carbonate rocks and the upper Paleozoic metasedimentary series is also tectonic in nature and corresponds to a decollement level located within the Silurian black schists. Talc and chlorite lenses crop out below this contact, discontinuously but all around the massif. From bottom to top, the Trimouns deposit is comprised of (Figs. 1c, 2a) a footwall of migmatites, micaschists, chloritized micaschists, and pure chlorite, the main talc ore, the hanging wall, made up of metasomatized dolostone, carbonates and schists from the Silurо-Ordovician series. Upper dolostone from this series contains REE minerals (Fig. 3a), particularly in the northern part of the hanging wall (Fig. 1c). In addition to these main units, the mineralization contains metric inclusions of pegmatites and micaschists. Rounded 2- to 10-m-sized pegmatite inclusions constitute tectonic clasts which are altered on their surface (Fig. 2b). The rim of the alteration contains allanite in the chlorite matrix (Fig. 3b) which could not be studied in this work because of their overconcentration in common lead. Micaschists inclusions constitute lenses that are tectonically detached from the footwall (Fortuné et al. 1980). Overall, the micaschists are more altered than the pegmatites.

In the Pyrenees, the association of talc and chlorite paragenesis is described almost exclusively in Trimouns (Fortuné 1971; Moine et al. 1982a, b; de Parseval 1992; de Parseval et al. 2004; Boiron et al. 2005). The chemical reaction leading to talc formation from dolostone alteration (east part of deposit—Fig. 1c) was described by de Parseval et al. (2004) as a combination of two reactions:

- dolostone alteration by silicium-charged fluid:

$$3CaMg(CO_3)_2 + 4SiO_2(aq) + 6H^+ = Mg_3Si_4O_{10}(OH)_2 + 3Ca^{2+} + 6CO_2 + 6H_2O$$

Fig. 2 Field relationships: **a** view of the Trimouns quarry, **b** chlorite from pegmatite, **c** chlorite from micaschists, chlorite in between marble boudins (hanging-wall veins) **d** at the Trimouns quarry. **e** Talc from Las Embollas and **f** chlorite from Col de Jau

- talc precipitation from percolating solution charged in silicium and magnesium:

$$4SiO_{2(aq)} + 3Mg^{2+} + 4H_2O = Mg_3Si_4O_{10}(OH)_2 + 6H^+$$

These two reactions can be simplified as:

$$2CaMg(CO_3)_2 + Mg^{2+} + SiO_2(aq) + 2H^+ = Mg_3Si_4O_{10}(OH)_2 + 2Ca^{2+} + 4CO_2$$

Talc formation involves an input of silicium and magnesium by the fluids. Ca and CO_2 leached out during the reaction could, respectively, form calcite which crystallizes in lower pressure zones (dolostone cavities) and hydrothermal graphite.

In Trimouns, chlorites are mostly clinochlore, a magnesium end member of chlorite solid solution (Wiewióra and Weiss 1990). They are formed by the alteration of silico-aluminous rocks such as pegmatites and micaschists (western part of the deposit—Fig. 1c). In both cases, chloritization requires an input of Mg and H_2O (Fortuné et al. 1980; de Parseval 1992) (Table 1). During the process of their alteration into chlorite (chloritization), the source rocks are depleted in many elements such as silicium and REE. These elements are then involved in the neoformation of a variety of hydrothermal minerals (xenotime, monazite allanite, etc.—Table 1). Titanium from the silico-aluminous rocks is

globally immobile and is consequently incorporated in the newly formed titanite or rutile crystals (de Parseval 1992). According to the metasomatic reactions described in their papers, Fortuné et al. (1980) and de Parseval (1992) proposed that the silicium leached during chlorite formation contributed to the formation of talc, so that chloritization and talcification are two complementary processes.

According to Boulvais et al. (2006), observations made on other carbonate-made talc–chlorite deposits in the Pyrenees, such as Col de Jau and Las Embollas (Fig. 1a), suggest a similar formation. They demonstrated that the oxygen and hydrogen isotope compositions are compatible with a marine origin for the fluids, although they were slightly modified by their interaction with the crustal rocks. The Col de Jau (Caillau quarry) and Las Embollas ores are located in the Axial Zone, a few tens of kilometers to the ESE of Trimouns (Fig. 1a). Similar to Trimouns, these deposits are formed at the contact between the Paleozoic-carbonated rocks and silico-aluminous rocks. The Col de Jau deposits lie in between the late Variscan Querigut and Milhas plutonic bodies (307 Ma for the Querigut pluton; Roberts et al. 2000). In the vicinity of the deposit, we can observe mylonitized granites, micaschists and associated hydrothermal chlorites. A marble layer with centimetric talc veins is also described. The ore is almost exclusively dominated by chlorite and more particularly clinochlore (Aranitis 1967). The Las Embollas deposit is located in the eastern part of the Villefranche syncline and is characterized by the presence of Devonian calcareous rocks (footwall) together with talc mineralization, while the hanging wall is made up of Visean schists. Talc is developed in the fault zones and contains calcareous elements (tectonic breccia—Aranitis 1967). The low magnesium content of the host rock suggests that the deposit has a hydrothermal origin (Raguin 1958). Chlorites are not described in the Las Embolas deposit.

Methodology

Sampling

The minerals dated by Schärer et al. (1999) came from a restricted part of the hanging wall of the Trimouns quarry and contained one monazite and four xenotime grains. As the talc ore does not contain minerals that can be directly dated, we sampled the chloritized rocks and talc–chlorite veins on both sides of the deposit which contain euhedral minerals such as titanite, rutile, xenotime, monazite and allanite that crystallized contemporaneously with the formation of talc and chlorite. All these minerals contain U and/or Th and can therefore be dated by the U–Th–Pb method (Poujol et al. 2010). Given the heterogeneity of the rocks affected by the metasomatism in the quarry (dolostone, schist, micaschists, gneiss and pegmatites), we sampled all the different lithologies present in the hanging wall and the footwall, from north to south of the quarry.

Microprobe

Quantitative analyses were performed at the University Toulouse III (GET Laboratory) using a CAMECA SX50 microprobe with SAMx automation. The operating conditions were: accelerating voltage 15 kV, beam current 10 or 20 nA (depending on the resistance of the mineral of beam damage), and analyzed surface $2 \times 2\ \mu m^2$. The following standards were used: fluorite (F), albite (Na), periclase (Mg), corundum (Al), tugtupite (Cl), sanidine (K), wollastonite (Ca), pyrophanite (Mn), hematite (Fe), chromium oxide (Cr), barite (Ba).

U–Th–Pb method

Ablation was performed at the University of Rennes I (Géosciences Rennes) using an ESI NWR193UC laser system powered by an ultrashort pulse Coherent ExciStar XS Excimer laser system operating at a wavelength of 193 nm and consisting of 7–70 µm spot diameters (depending on the size and nature of the mineral) produced with a repetition rate of 3–4 Hz and a fluence of 8 J/cm^2. Ablated material was carried to the mass spectrometer in He and then mixed with N and Ar before being introduced to the ICP source of an Agilent 7700× quadrupole ICP–MS equipped with a dual pumping system to enhance sensitivity (Paquette et al. 2014). Tuning of the instrument and mass calibration were performed before the analytical session using the NIST SRM 612 reference glass, by monitoring the ^{238}U signal and minimizing the ThO+/Th+ ratio (<0.5 %). The analyses consisted of the acquisition of the ^{204}(Pb + Hg), ^{206}Pb, ^{207}Pb, ^{208}Pb, ^{232}Th and ^{238}U signals. The ^{235}U abundance was calculated from the measured ^{238}U on the basis of a $^{238}U/^{235}U$ ratio of 137.88. Single analyses consisted of ~20 s of background integration with the laser off, followed by ~60-s integration with the laser firing and then a ~10-s delay for wash out. The analyses were performed in time-resolved mode.

Raw data were corrected for Pb/U and Pb/Th laser-induced elemental fractionation and for instrumental mass discrimination by standard bracketing with repeated measurements of different standard reference materials: GJ-1 for titanite and allanite dating (Jackson et al. 2004);

Table 1 Adapted from de Parseval et al. (2004)

infiltration ←			
Source rock	**Intermediate zone**		**Ore**
Micaschists and pegmatites: - *quartz* - *plagioclase*, - *muscovite* - *accessories minerals*	**Phlogopite zone**: - *quartz* - *phlogopite* - *muscovite* - *(+/-) chlorite* - *accessories minerals*	**Quartz-chlorite zone**: - *quartz* - *chlorite* - *(+/-) phlogopite* - *accessories minerals*	**Chlorite ore**: - *chlorite*, - *(+/-) talc* - *accessories minerals*
	+Mg, + H2O *-Na, -K, -Ca, -Si* *globally inert Al, Fe, Ti, P*		
Dolostones: - *dolomite* - *accessories minerals*	**no intermediate zone**		**Talc ore**: - *talc* - *(+/-) chlorite* - *accessories minerals*
	+Si, *-Ca, -CO2*		

Source to ore at Trimouns quarry according to hydrothermalism degree

Moacir for monazite (Gasquet et al. 2010); Weinsberg for xenotime (Klötzli et al. 2007) and R10 for rutile (Zack et al. 2011). Both standards—LAC titanite (Pedersen et al. 1989) and Bona and Tera allanite (Gregory et al. 2007)—available in Geosciences Rennes contain a non-negligible proportion of common Pb. As both titanite and allanite are silicates, we decided to use the GJ-1 zircon as the primary standard. As already explained in Fallourd et al. (2014), Sun et al. (2012) claimed that titanite can be up to 12 % younger than their known ages using either spot or raster analyses when a zircon standard is used. However, Storey et al. (2006) and Darling et al. (2012) concluded that the error related to the non-matrix matching between the unknown (titanite and allanite, respectively) and the external standard (zircon) is negligible. The systematic analyses of the matrix-matching standards (treated as unknown) during the course of the analyses demonstrated that this approach is valid.

With the samples, other standards were measured as unknowns to monitor the precision and accuracy of the analyses: titanite from the Lillebukt alkaline complex in northern Norway (ca. 520 Ma; Pedersen et al. 1989); 516.4 ± 5.5 Ma (N = 28), MSWD = 3.4); Bona and Tara allanite (ca. 31 and 418 Ma; Gregory et al. 2007); 30 ± 4 Ma (n = 9, MSWD = 2) and 429 ± 35 Ma (n = 8, MSWD = 5.3); Manangoutry monazite (ca. 555 Ma; Paquette and Tiepolo 2007); 561 ± 8 Ma (n = 8), MSWD = 1.9) and rutile R19 (ca. 490 Ma; Zack et al. 2011); 481 ± 9 Ma (n = 14), MSWD = 5.3). Data reduction was carried out with the GLITTER software package (Van Achterbergh et al. 2001).

Sample descriptions

Trimouns

From the footwall to the hanging wall, we sampled three types of rocks containing REE and titanium-rich minerals:

- Chloritized micaschists (footwall and main ore—Fig. 2c) which contain titanium-rich minerals in the chlorite matrix (details in Table 2). Samples P101, P248 and Z103E are localized in the northern part of the ore (Fig. 1c). Sample Gis10 is the closest to the talc mineralization.
- Geodes from massive dolostones (REE mineral zone—Fig. 1c) which contain xenotime, monazite, allanite and rutile, in a dolomitic matrix (Fig. 3a). These cavities are often filled with talc. The seven samples are listed in Table 2.
- Decametric chlorite veins in the hanging wall, which are developed in pressure shadows between marble boudins formed by the Paleozoic series (Fig. 2d). They contain chlorite, titanite (ca. 2 cm), calcite and pyrite. Sample Toi9a (Fig. 3d) is a chlorite vein which contains euhedral titanite surrounded by calcites and chloritites. Sample Toi9b (Fig. 3c) is a chlorite vein which contains anhedral/alterated titanite exclusively surrounded by chlorite.

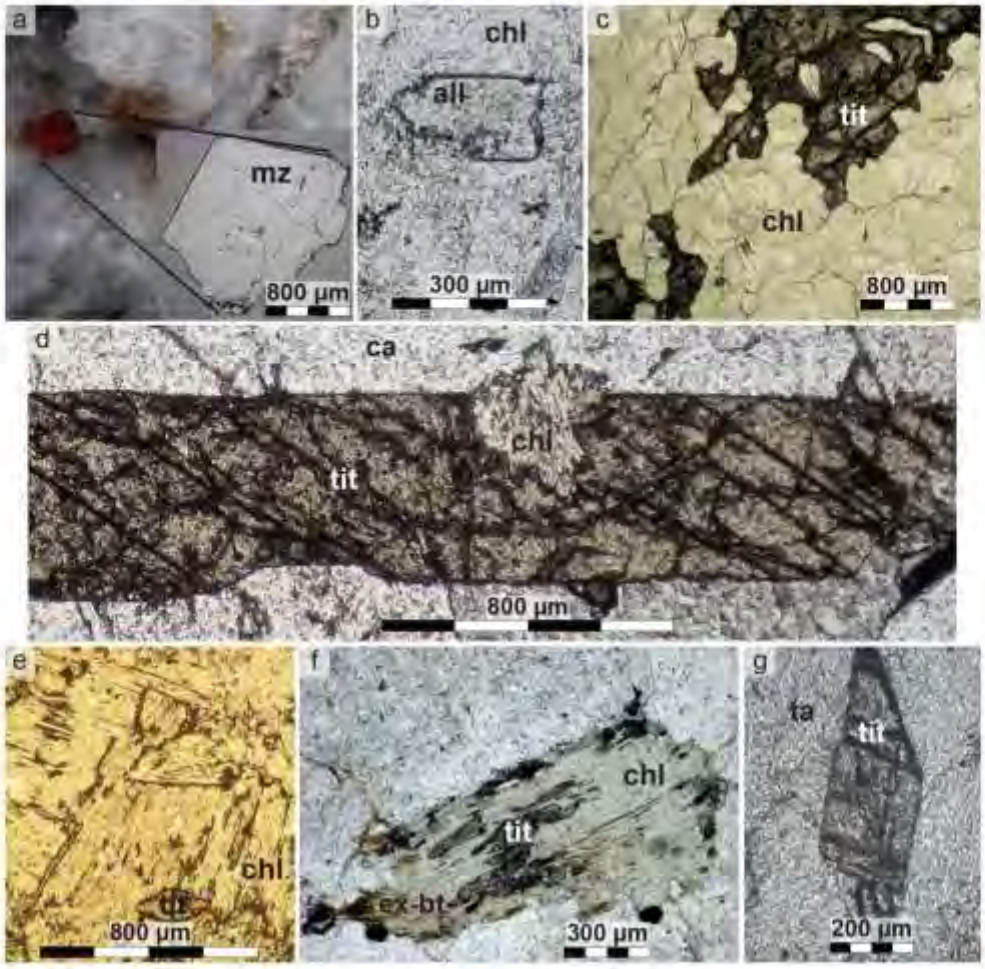

Fig. 3 Microscopic view of the minerals sampled. Trimouns: **a** monazite (*mz*) in dolostone geodes, macro- and SEM view, **b** hydrothermal allanite (*all*) in chloritized pegmatite, **c** anhedral titanite (*tit*) and **d** euhedral titanite from chlorite (*chl*) mineralization. Col de Jau: **e** hydrothermal isolated titanite in chlorite mineralization and **f** hydrothermal titanite in a biotite/chlorite assemblage (*ex-bt*). Las Embollas: **g** hydrothermal titanite in talc mineralization

Col de Jau

The Col de Jau deposit is essentially comprised of chlorite and is developed at the expense of micaschists and granite (Aranitis 1967; Boulvais et al. 2006). We sampled the chlorite vein and its partially altered granitic host rocks (details in Table 2):

- Altered granite: sample Jau00-87, which contains titanite in a biotite/chlorite assemblage.
- Chlorite vein: sample Jau00-89, essentially comprised of chlorite. Some euhedral titanite grains are isolated in the matrix (Fig. 3e).
- Jau00-96 represents a contact between chlorite and altered granite. Titanite grains are associated with quartz in the altered zone, but are not in contact with chlorite.

Las Embollas

In the Las Embollas deposit, which is exclusively made up of talc, we sampled talc veins in contact with the carbonated rock (sample Emb01-179B). We observed only one type of titanite in the talc veins (Fig. 3g).

Table 2 Samples location coordinates, description of rock and nature of minerals date

Site	Sample name	Type	Minerals dated	GPS coordinate	
Trimouns					
Footwall	P248	Chloritized footwall	Euhedral titanite	42°48.540′N	1°48.073′E
Main ore	Gis10	Chlorite from micaschists "inclusion"	Titanite and rutile	42°48.497′N	1°48.039′E
Main ore	P101	Chloritite	Euhedral titanite	42°48.867′N	1°48.254′E
Main ore	Z103E	Chloritite	Euhedral titanite	42°48.611′N	1°48.203′E
Hanging wall	GB2	Geode in dolostone	Euhedral monazite	42°48.735′N	1°48.337′E
Hanging wall	GB3	Geode in dolostone	Euhedral xenotime	42°48.735′N	1°48.337′E
Hanging wall	Toi10	Geode in dolostone	Euhedral xenotime	42°48.683′N	1°48.300′E
Hanging wall	Toi10.0	Geode in dolostone	Euhedral allanite	42°48.683′N	1°48.300′E
Hanging wall	Toi10.2	Geode in dolostone	Euhedral xenotime	42°48.683′N	1°48.300′E
Hanging wall	Toi10.4	Geode in dolostone	Euhedral rutile	42°48.683′N	1°48.300′E
Hanging wall	Toi27	Geode in dolostone	Euhedral monazite	42°48.641′N	1°48.276′E
Hanging wall	Toi9a	Chlorite veins	Euhedral titanite	42°48.365′N	1°48.177′E
Hanging wall	Toi9b	Chlorite veins	Anhedral titanite	42°48.365′N	1°48.177′E
Col de Jau					
	JAU00-87	Granite altered	Euhedral titanite	42°40.040′N	2°14.668′E
	JAU00-89	Chlorite from micaschists	Euhedral titanite	42°40.040′N	2°14.668′E
	JAU00-96	Chlorite and altered granite	Euhedral titanite	42°40.040′N	2°14.668′E
Las Embollas					
	EMB01-179B	Talc vein	Euhedral titanite	42°35.059′N	2°22.892′E

Results

U–(Th)–Pb analysis

In this part, we present the results obtained by LA ICP–MS on the REE minerals or titanium-rich minerals described in the previous sections. For the samples from the Trimouns deposit, with the exception of monazite (sample GB2 and Toi27), all the results are plotted in Tera–Wasserburg diagrams. For the monazite, the data are plotted in $^{206}Pb/^{238}U$ vs $^{208}Pb/^{232}Th$ concordia diagrams (Poujol et al. 2010) (Fig. 4m, n). Col de Jau and Las Embollas are plotted in Tera–Wasserburg diagrams (respectively, Fig. 4o, p). BSE imaging of the dated minerals shows that they are unzoned.

Trimouns footwall

- Sample Gis10: Two types of minerals were analyzed:
  1. One euhedral titanite (two fragments) with 24 spots (Fig. 4a). All the analyses are very discordant and define a discordia with a lower intercept at of 98.5 ± 1.7 Ma (MSWD = 2). The upper intercept is compatible with the composition of a common Pb at ca. 100 Ma following the model of Stacey and Kramers (1975) for the Pb evolution. If we forced the discordia to this composition, we obtain a similar date of 98.7 ± 1.5 Ma (MSWD = 1.9). We interpret this date of ca. 98 Ma as the age of crystallization for this titanite.
  2. One euhedral rutile (three fragments) with 17 spots. These analyses also plot in a discordant position, although they are slightly less discordant than the titanite and allow to draw a discordia with a lower intercept at 103.4 ± 3 Ma (MSWD = 3.2) (Fig. 4b). As for the titanite, the upper intercept is compatible with the composition of a common Pb at ca. 100 Ma (Stacey and Kramers 1975). If the discordia is forced to that composition, we obtain a similar date of 103.8 ± 3.1 Ma (MSWD = 3). This date is interpreted as the crystallization age of the rutile.
- Sample P101: On the same thin section, 14 titanite grains were analyzed with 21 spots (Fig. 4c). They plot in a discordant position and define a discordia with a lower intercept at 166.1 ± 9.4 Ma (MSWD = 2.2). If the discordia is forced to the common Pb composition at ca. 165 Ma according to Stacey and Kramers (1975), we obtain a similar date of 167.3 ± 7.8 Ma (MSWD = 2.1) interpreted as the crystallization age for these titanite grains.
- Sample P248: Nine spots were analyzed within five different titanite grains. A regression through these discordant analyses gives a lower intercept at 167 ± 38 Ma (MSWD = 5.9) (Fig. 4d) compatible within error with

the date of 157 ± 37 Ma (MSWD = 5.6) obtained if the discordia is forced to a common Pb composition calculated at ca.165 Ma according to the model of Stacey and Kramers (1975). Although poorly constrained, we conclude that this date of ca. 160 Ma represents the crystallization age of these titanite grains.

- Sample Z103E: 16 spots on 10 titanite grains were analyzed in the same thin section (Fig. 4e). The data plot in a discordant position and define a discordia with a lower intercept at 166.5 ± 4.2 Ma (MSWD = 1.3) identical to the date of 166.5 ± 4.2 Ma (MSWD = 1.17) if forced to the common Pb composition at ca. 165 Ma (Stacey and Kramers 1975). This Jurassic date is interpreted as the crystallization age of these titanite grains.

Trimouns hanging wall

- Sample Toi9 a & b:
  1. For Toi9a, one centimetric euhedral titanite (Fig. 3d) from the chlorite veins in the hanging wall was analyzed (20 spots) in the thin section (Toi9a—Fig. 4f). The data define a discordia with a lower intercept date of 98.3 ± 2.8 Ma (MSWD = 2) identical within error to the date of 98.5 ± 2.7 Ma (MSWD = 3.4) obtained if the discordia is anchored to a common Pb composition calculated at 100 Ma according to the model of Stacey and Kramers (1975). This date of ca. 98 Ma is interpreted as the crystallization age of this titanite.
  2. For Toi9b, one centimetric anhedral titanite (Fig. 3c) was analyzed (20 spots) in the thin section (Toi9b—Fig. 4g). Discordant to very discordant data define a lower intercept date of 99.6 ± 1.7 Ma (MSWD = 1.2). This date is indistinguishable from the date of 99.6 ± 1.7 Ma (MSWD = 1.16) if the discordia is forced to the common Pb composition calculated at ca. 100 Ma (Stacey and Kramers 1975). This date of ca. 99 Ma is interpreted as the crystallization age of this titanite.
- Sample Toi10.4: One centimetric euhedral rutile was analyzed (five spots). The data plot in a discordant position and define a lower intercept date of 96.6 ± 4.4 Ma (MSWD = 1.2; Fig. 4h). If the discordia is forced to the common Pb composition calculated at ca. 100 Ma (Stacey and Kramers 1975), we obtain a similar date of 96.8 ± 4.6 Ma (MSWD = 0.96). This date of ca. 97 Ma is interpreted as the crystallization age of this rutile.
- Sample Toi10.0: Five euhedral allanite grains from the same geode in dolostone were analyzed (21 spots). All the data points are discordant, but they fit on a discordia pointing to a lower intercept at 119.6 ± 4.8 Ma (MSWD = 2.4) (Fig. 4i). This date is similar to the date of 119.5 ± 5.3 Ma (MSWD = 2.2) obtained if the regression is forced to the composition of common Pb calculated following the model of Stacey and Kramers (1975). We conclude that these allanite grains crystallized ca. 119 Ma ago.
- Sample GB3: One euhedral xenotime divided into two fragments was analyzed (14 spots). Plotted in a concordia diagram, the data are concordant to discordant. If we do not take the four most discordant analyses into account (shown as a dashed line in Fig. 4j), we can calculate a concordia date of 111.07 ± 0.96 Ma (MSWD = 0.83) that is confirmed by the weighted mean $^{206}Pb/^{238}U$ date of 111.2 ± 0.76 Ma (MSWD = 0.19) calculated for all the data. Therefore, we consider that this xenotime crystallized ca. 111 Ma ago.
- Sample Toi10: One euhedral xenotime was analyzed (10 spots). All the data except for three (shown as a dashed line in Fig. 4k) plot in a concordant position and can be used to calculate a concordia date of 122 ± 1.4 Ma (MSWD = 1.2). This date is in a good agreement with the weighted mean $^{206}Pb/^{238}U$ date of 121.7 ± 1.1 Ma (MSWD = 0.27) obtained with all the data. We therefore conclude that this xenotime crystallized ca. 121 Ma ago.
- Sample Toi10.2: One euhedral xenotime was analyzed (28 spots). Plotted in a concordia diagram (Fig. 4l), all the data are concordant within error. The resulting concordia date is 111.02 ± 0.46 Ma (MSWD = 0.64) which is interpreted as the crystallization age for this xenotime.
- Sample GB2: One euhedral centimetric monazite was analyzed (18 spots). All the data plotted in a $^{206}Pb/^{238}U$ versus $^{208}Pb/^{232}Th$ concordia diagram (Fig. 4m) are concordant within error and can be used to calculate a concordia date (Ludwig 1998) of 102.64 ± 0.65 Ma (MSWD = 1.2) that we interpret as the crystallization age of this monazite grain.
- Sample Toi27: Six euhedral centimetric monazite grains were analyzed (21 spots). In a $^{206}Pb/^{238}U$ versus $^{208}Pb/^{232}Th$ concordia diagram (Fig. 4n), they all plot, within error, in a concordant position and can be used to calculate a concordia date of 104.64 ± 0.56 Ma (MSWD = 1.06) that we consider as the crystallization age for these monazite grains.

Fig. 4 Tera–Wasserburg concordia diagrams for **a** titanite and **b** rutile from sample Gis10 and for titanites from samples **c** P101, **d** P248, **e** Z103E, **f** Toi9a. From sample **g** Toi9b, rutile from sample **h** Toi10.4, allanite from sample **i** Toi10.0, and xenotimes from samples **j** GB3, **k** Toi10, **l** Toi10.2. Concordia diagram ($^{206}Pb/^{238}U$–$^{208}Pb/^{232}Th$) for monazites from samples **m** GB2 and **n** Toi27, **o** titanite from Col de Jau (JAU00-87, JAU00-89, & JAU00-96) with two age trends and for **p** titanite from Las Embollas (EMB01-179B)

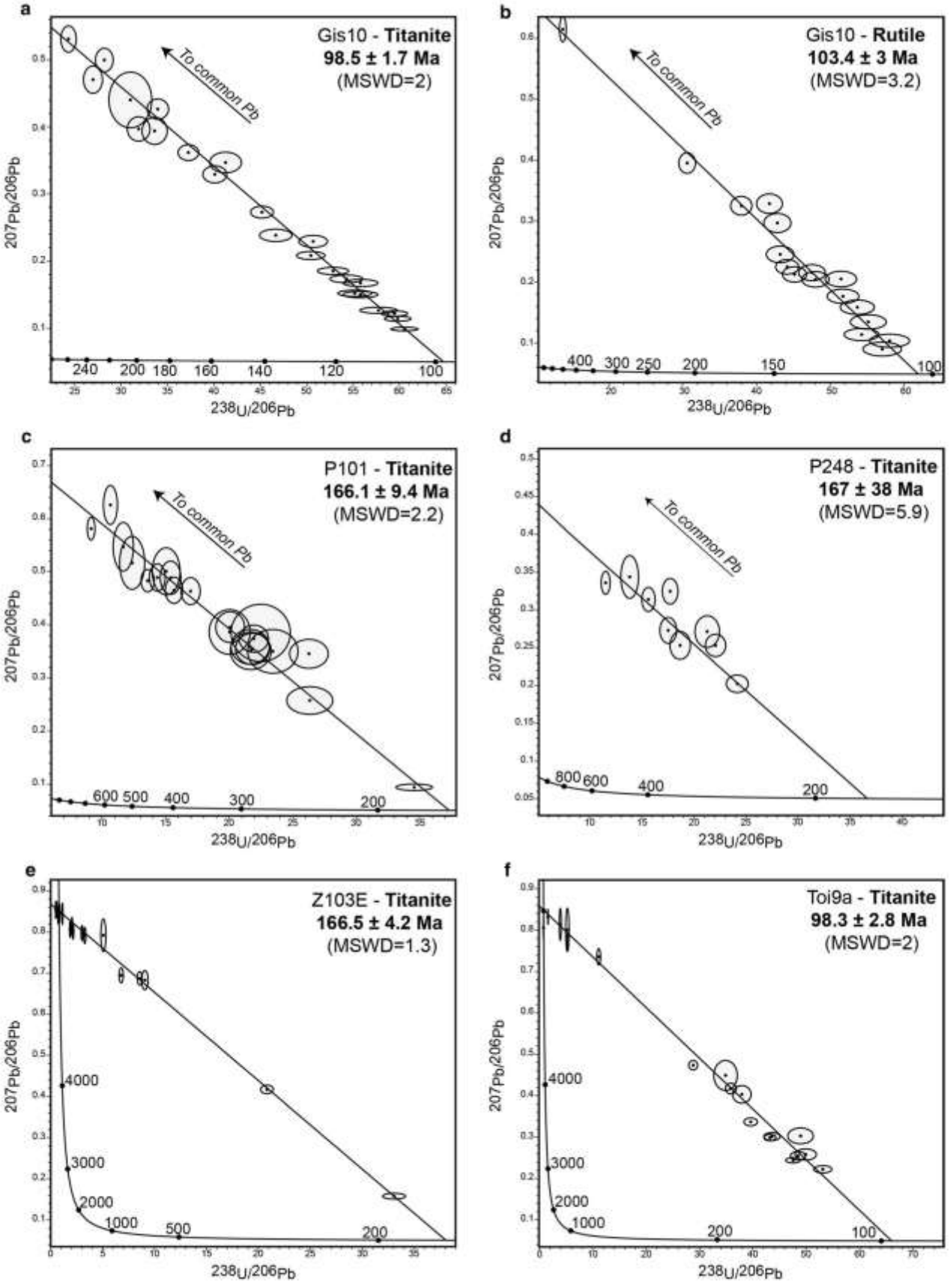
a
Gis10 - Titanite
98.5 ± 1.7 Ma
(MSWD=2)
To common Pb
240 200 180 160 140 120 100
b
Gis10 - Rutile
103.4 ± 3 Ma
(MSWD=3.2)
To common Pb
400 300 250 200 150 100
c
P101 - Titanite
166.1 ± 9.4 Ma
(MSWD=2.2)
To common Pb
600 500 400 300 200
d
P248 - Titanite
167 ± 38 Ma
(MSWD=5.9)
To common Pb
800 600 400 200
e
Z103E - Titanite
166.5 ± 4.2 Ma
(MSWD=1.3)
4000 3000 2000 1000 500 200
f
Toi9a - Titanite
98.3 ± 2.8 Ma
(MSWD=2)
4000 3000 2000 1000 200 100
207Pb/206Pb
238U/206Pb

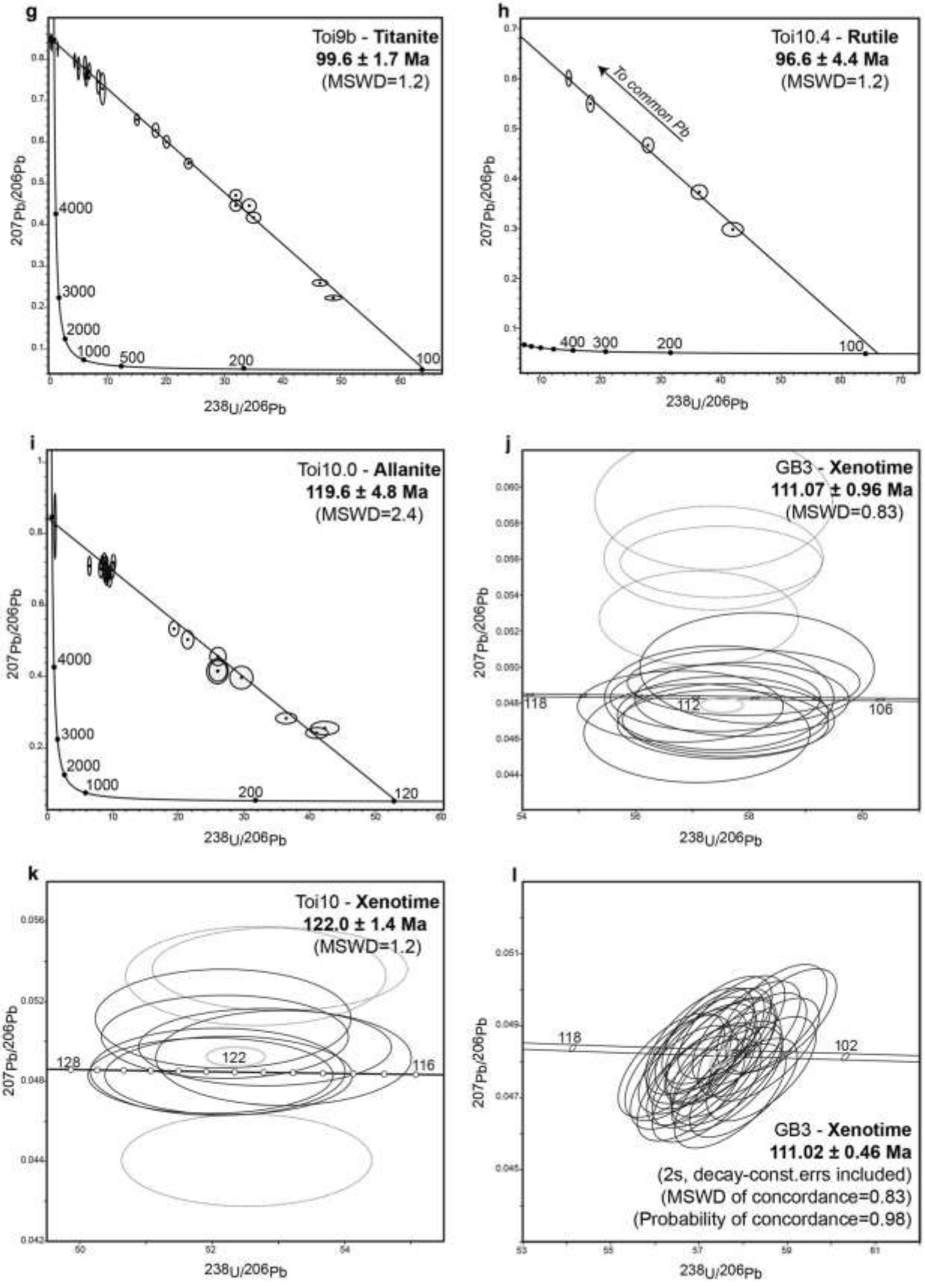

Fig. 4 continued

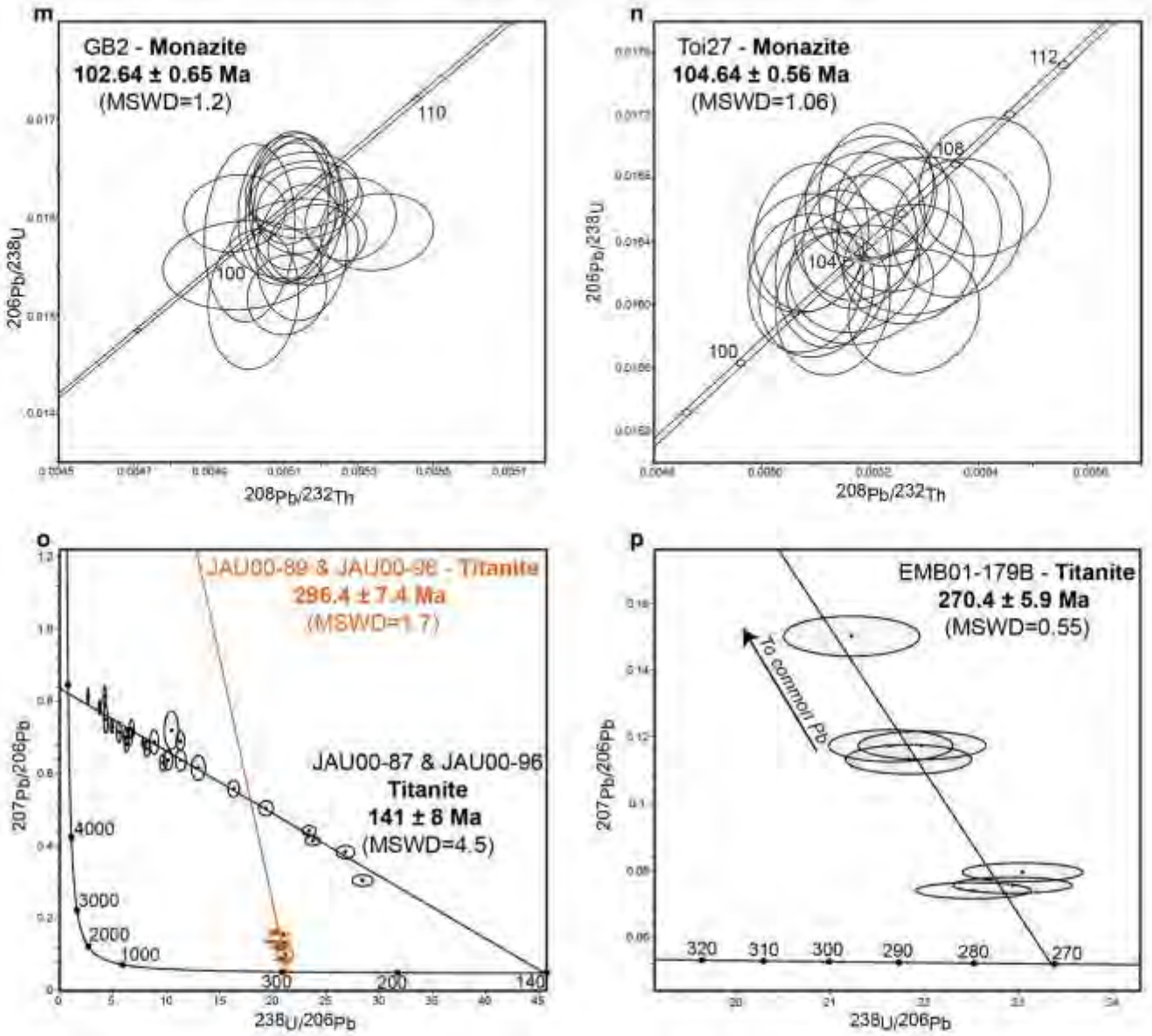

Fig. 4 continued

Col de Jau

- Sample JAU00-87: 12 euhedral titanite grains were analyzed (22 spots). Together with three spots from JAU00-96 (see below), the data are discordant but define a lower intercept age of 141 ± 8 Ma (MSWD = 4.5) (Fig. 4o). If the discordia is forced to the common Pb composition at ca. 140 Ma according to Stacey and Kramers (1975), we obtain a similar date of 141 ± 7.8 Ma (MSWD = 4.3), interpreted as the crystallization age for these titanite grains.
- Sample JAU00-89: Two euhedral titanite grains were analyzed (five spots). Together with five spots from JAU00-96 (see below), the data are slightly discordant and define a lower intercept date of 296.5 ± 7.5 Ma (MSWD = 1.6). There is however no possibility to calculate a date if the discordia is forced to the common Pb composition at ca. 300 Ma. This can be explained by a Pb loss for at least the most discordant points. This type of Pb loss will move the points toward the right of the diagram, parallel to the $^{238}U/^{206}Pb$ axis and will result in an anomalously "old" upper intercept (i.e., an anomalously $^{207}Pb/^{206}Pb$ value that is too high for common Pb). Therefore, this date of ca. 296 Ma should be interpreted as the minimum crystallization age for these titanite grains.
- Sample Jau00-96: Three euhedral titanite grains were analyzed (eight spots). The data plot in a discordant position and do not define a simple trend. However, grains 1, 2 and 3 fit on the discordia defined by the anal-

yses on the titanite grains from sample Jau00-87 (see above), while the other analyses (grains 4–8) fit on the discordia obtained with the titanite grains analyzed in sample Jau00-89 (see above).

Las Embollas

- Sample Emb01-179B: One euhedral titanite was analyzed (seven spots). In a concordia diagram, the data are slightly discordant and define a lower intercept date of 270.4 ± 5.9 Ma (MSWD = 0.55) (Fig. 4p). If the discordia is forced to the common Pb composition at 270 Ma following the model of Stacey and Kramers (1975), the lower intercept age is identical within error at 269 ± 5.2 Ma (MSWD = 0.63). We therefore consider that this titanite crystallized ca. 270 Ma ago.

Chemical compositions of chlorite

In the previous section, we obtained three different ages for the chloritization in Trimouns, Col de Jau and Las Embollas: i.e., Permian, Jurassic and Cretaceous. As the hydrothermal chlorite composition is controlled by the nature of the host rock and the composition of the fluids responsible for the chloritization, it is important to check whether there is a correlation between the chlorite compositions and the ages of chloritization. Because all the chlorite crystals encountered in the ore deposits are ferromagnesian, we plotted the chlorite compositions in a ternary diagram (clinochlore + daphnite–amesite–sudoïte) according to the chlorite classification (Wiewióra and Weiss 1990) and the work of Vidal et al. (2001).

Trimouns

- Samples from the main chlorite ore (Fig. 5a): de Parseval (1992) demonstrated that chlorite from the Trimouns main ore is either clinochlore or daphnite. On the four samples used for dating (Gis10, P101, Z103E and P248), 12 chlorite crystals were analyzed with an electron microprobe. The compositions of these crystals are within the average for chlorite compositions at the scale of the main ore. No correlation can be established between the ages and the chlorite compositions.
- Samples from the hanging-wall vein: 33 chlorite crystals from samples Toi9a and Toi9b were analyzed. The compositions are different from the ones found for the main chlorite ore, as they plot closer to the amesite pole and further away from the clinochlore + daphnite pole (Fig. 5b). This difference can mainly be explained by the lithological difference between the host rocks: marble in the case of Toi9 samples and micaschists for the samples from the main chlorite ore.

Col de Jau

All 32 chlorite crystals analyzed from the Col de Jau deposit plot close to the chlorite compositions found for the Trimouns main ore (Fig. 5c). As the compositions are similar in Col de Jau and in Trimouns (main ore), no correlation can be established between the chlorite compositions and the ages.

Considering all these results, we cannot establish a correlation between the mineralization ages and the chlorite compositions, but instead find a correlation between the

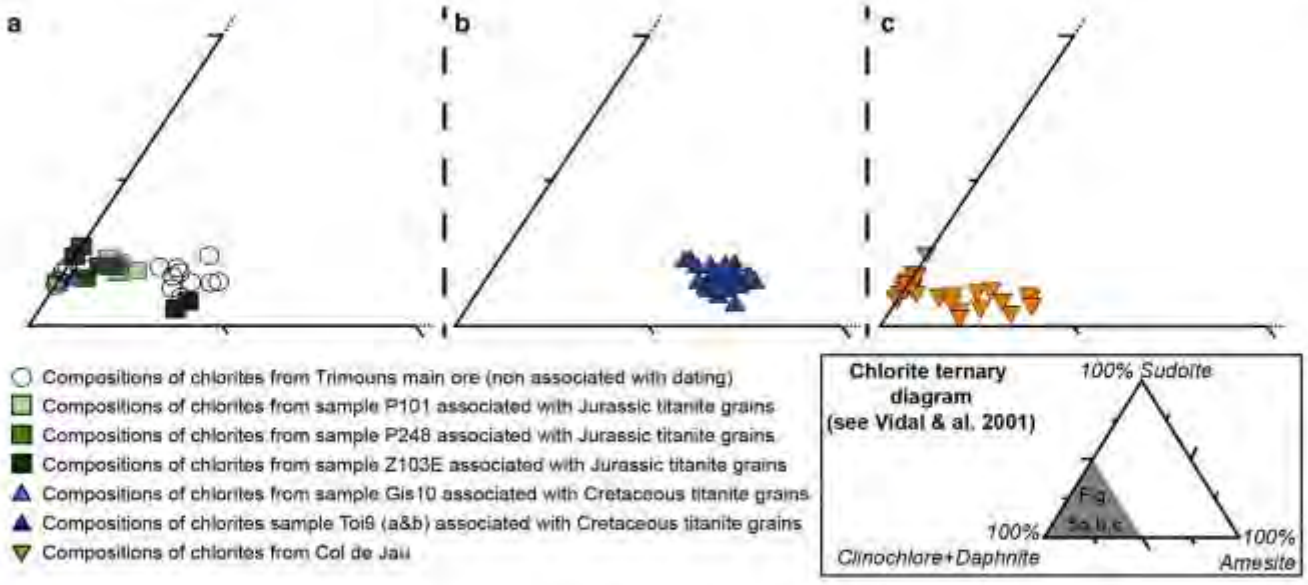

Fig. 5 Chlorite ternary diagram of **a** the Trimouns main ore, **b** the Trimouns chlorite veins in the hanging wall and at **c** Col de Jau

chlorite and protolith compositions. As the chlorite composition is related to the protolith composition as well as to the composition of the metasomatic fluids, this seems to show that the general context for the fluid circulation during the chloritization metasomatic events was similar from the Permian to the Cretaceous.

Discussion

Age interpretation

In Trimouns, the chlorite mineralization contains euhedral titanite and rutile which were formed by metasomatic alteration during the leaching of the footwall micaschists (Fortuné et al. 1980; de Parseval 1992). Therefore, it is reasonable to interpret the ages obtained from in situ U–Pb dating of these minerals as the ages of their crystallization. Thus, we consider that the dates we obtained from titanite and rutiles in chloritites are the ages of the chloritization event(s). The temporal relationship between the chloritization and talc formation could not clearly be established with these data only.

In contrast, as demonstrated by Schärer et al. (1999) and de Parseval (1992), the minerals found within the geodes in the dolostones (REE-rich minerals and rutile) are contemporaneous with both the talcification and chloritization processes because all the REE minerals crystallized from the hydrothermal fluids responsible for talc and chlorite formation. The REE in the fluids most likely results from the leaching of the micaschists and more particularly by the dissolution of the accessory allanite crystals present in the underlying micaschists, taking place simultaneously with their alteration to chlorite (de Parseval et al. 1997). This is corroborated by the P–T conditions that prevailed during the hydrothermal activity in Trimouns, which did not exceed a temperature of 250–300 °C and a pressure between 0.2 and 0.3 GPa (Boiron et al. 2005). These P–T conditions correspond to the condition of hydrothermal growth of the xenotime, monazite and allanite crystals. For these REE minerals, as no inheritance has been found (this work; Schärer et al. 1999), and because they are in textural equilibrium with the talc in the dolostone cavities, we are confident that the obtained ages represent the age of both the crystallization of the REE minerals and the formation of the talc and chlorite ores.

We thus consider that all the ages we have obtained on the euhedral minerals in the samples from the chloritized micaschists in the footwall and from the chlorite–talc veins and geodes in the hanging wall, can be interpreted as representative of the ages of the chloritization and talcification events.

In the Las Embollas deposit, because of their textural position, the titanite grains found in the talc vein seem to have crystallized during veining. We thus consider that the Permian ages obtained for the titanite crystallization date the talcification event.

Using the same arguments, the titanite grains contained in the chlorite (samples Jau00-87 and Jau00-89) from the Col de Jau deposit are considered as contemporary to the formation of the chlorites. For the titanite in the quartz from sample Jau00-96, we obtained two age trends with the same type of titanite texture. These trends are superposed with dating from Jau00-87 or Jau00-89. In this case, we consider that the two generations of titanite are associated with two distinct hydrothermal events which led to quartz precipitation. This quartz formation can thereafter be associated with the chloritization event recorded by samples Jau00-87 and Jau00-89.

The polyphased formation of the Trimouns deposit

The talc and chlorite mineralization found in the Trimouns deposit was classically interpreted to be the result of a single mineralizing event that produced both talc and chlorite (Fortuné 1971; Fortuné et al. 1980; Moine et al. 1982a, b; de Parseval 1992; Boulvais et al. 2006). Accordingly, Schärer et al. (1999) interpreted their monazite and xenotime ages as representative of a single Albian chlorite and talc mineralization event. In this study, we dated minerals associated with both chlorite and talc mineralization, in the footwall and in the hanging wall of the Trimouns deposit. We demonstrate the existence of at least two distinct mineralization events in Trimouns. The oldest is Jurassic (ca. 165 Ma), corresponds to a chloritization event and is only recognized near the footwall of the main ore zone. The youngest is a talc–chlorite mineralization event and ranges from the Aptian to the Cenomanian (ca. 121–96 Ma). It is recorded in the hanging wall and in the main ore close to the chloritized footwall.

Cretaceous talc and chlorite mineralization

Our data show that the ages for the talc–chlorite mineralization range from Aptian up to Cenomanian. The ages from the minerals found in the dolostones range from ca. 121 Ma down to ca. 96 Ma: (1) The Aptian ages were obtained on allanite (119.6 ± 4.8 Ma) and xenotime (121.7 ± 1.1 Ma) from sample Toi10.0. (2) A second, slightly younger Albian age was obtained on xenotime from two samples (sample GB3: 111.2 ± 0.4 Ma and sample Toi10.2: 110.8 ± 0.5 Ma). (3) Monazite from two samples gave Albian ages of 104.6 ± 0.6 Ma (Toi27) and 102.6 ± 0.7 Ma (G2), respectively. (4) Finally, rutile

from sample Toi10.4 Ma gave a Cenomanian age of 96.6 ± 4.4 Ma. According to these results, it seems that the crystallization order was, from older to younger, allanite/xenotime, then monazite and finally rutile. These results suggest a protracted period for the mineral crystallization in the dolostone cavities and talc veins. If we consider that our sampling is representative of the whole mineralization event, we consider that this apparent crystallization order could be the consequence of (1) variations in the fluid composition (Si activity, REE and/or volatile contents) (2) and/or fluid temperature.

The ages from the samples located in the chloritized zone in the hanging wall and in the main ore (close to the footwall) are all clustered around 100 Ma: (1) Titanite grains from sample Toi9 in the hanging wall gave an Albo-Cenomanian age of, respectively, 98.3 ± 2.8 Ma (euhedral mineral—Toi9a) and 99.6 ± 1.7 Ma (anhedral mineral—Toi9b). (2) Titanium-rich minerals from sample Gis10 in the main ore (near the footwall) gave an Albo-Cenomanian age of 98.5 ± 1.7 Ma on titanite and 103.4 ± 3 Ma on rutile. These results confirm that titanium was present in the hydrothermal fluid and incorporated in titanite or rutile until the end of the Cretaceous hydrothermal event.

Depending on how we take the individual errors into account, we are able to identify a duration of about 25–30 Ma for the fluid circulation event(s) responsible for the Cretaceous talcification and chloritization event. This time interval is slightly longer than the 112- to 97-Ma interval proposed by Schärer et al. (1999). As our sampling is representative of the various lithologies and of the whole structural section of the deposit, the ages and duration we discussed above are significant at the scale of the deposit. Although we cannot exclude that this fluid circulation event was continuous during this period of time, our dataset seems to be more compatible with a pulse-driven activity. Indeed, we can identify two limited fluid pulses around 120 and 110 Ma, which occurred before the major fluid pulse at ca. 100 Ma. This last pulse could be related, at a regional scale, to a warmer fluid circulation event occurring around 100 Ma as described by Fallourd et al. (2014) for the alkali metasomatism. This Na–Ca metasomatic event is slightly younger (110–92 Ma) and warmer (ca. 550 °C) than the Na metasomatism (ca. 117–98 Ma and 350–450 °C). Consequently, the Na–Ca metasomatism and the late stage of the talc–chlorite event could be synchronous with the Cretaceous Pyrenean Metamorphism at ca. 105–85 Ma (Albarède and Michard-Vitrac 1978; Montigny et al. 1986; Golberg and Leyreloup 1990) and therefore to an advanced stage of crustal thinning. However, this hypothesis does not imply that such high temperature fluids have actually circulated at the Trimouns site; Boiron et al. (2005) did not identify such "hot" fluids. These fluids may well have been generated deeper in the crust and cooled during their migration toward the Trimouns site, triggering a new generation of metasomatic alteration in the upper structural levels. Even if these late fluids may have presented slight distinct chemical properties, stabilizing rutile rather than other minerals, it is very unlikely that its U–Pb system has been disturbed by the late Cretaceous hydrothermal activity.

Jurassic chlorite mineralization

Some samples from the chloritite found close to the footwall gave Jurassic ages. These three samples from the northern part of the Trimouns deposit provided titanite crystallization ages of 166.1 ± 9.4 Ma, 166.5 ± 4.2 Ma and 167 ± 38 Ma, respectively. These ages are identical within error. Sample P248 (167 ± 38 Ma) yielded scattered data with a high MSWD (Fig. 4d); we do not include this age in the "Jurassic event" window in Fig. 6a, although it is identical within error to the two previous ones.

All these ages concern minerals found in the chloritized zone and near the footwall. No Jurassic ages were found in the source rock of the talc mineralization, i.e., the dolostones. This could be explained by two hypotheses: (1) Only chlorite was formed during the Jurassic event, or (2) the Jurassic event produced both talc and chlorite, but the Jurassic talc was removed. Because we are confident that our sampling, which is based on a recent precise mapping (Boutin et al. in prep.) and on deep and detailed knowledge of the deposit, is representative of the whole history of the Trimouns ore, we propose that the first hypothesis is by far more likely, i.e., there was no talc formation during the Jurassic event.

If we consider that the Jurassic mineralizing event was only responsible for chloritization, this implies that the elements needed to form talc were either not present or in insufficient quantities in the fluid. This scenario could be explained by different hypotheses (non-exhaustive list): (1) not enough magnesium and/or silicium in the hydrothermal fluid to form talc during the Jurassic event (see the chemical equation in the geological context). (2) In this period, the dolostones were not in contact with the chloritized micaschists. These carbonated rocks could have been brought on top of the micaschists by tectonic movements after the Jurassic and before (or during) the onset of the Cretaceous mineralization event. (3) The dolomitization of the calcic Paleozoic series happened after the Jurassic event and at the beginning of the Cretaceous event. This last hypothesis was also proposed by Boulvais et al. (2006) and suggests that a very large input of magnesium was necessary to produce both dolomitization and talcification. This could be related to the mantle exhumation and associated serpentinization recently evidenced in the area (Lagabrielle et al. 2010; Clerc et al. 2012).

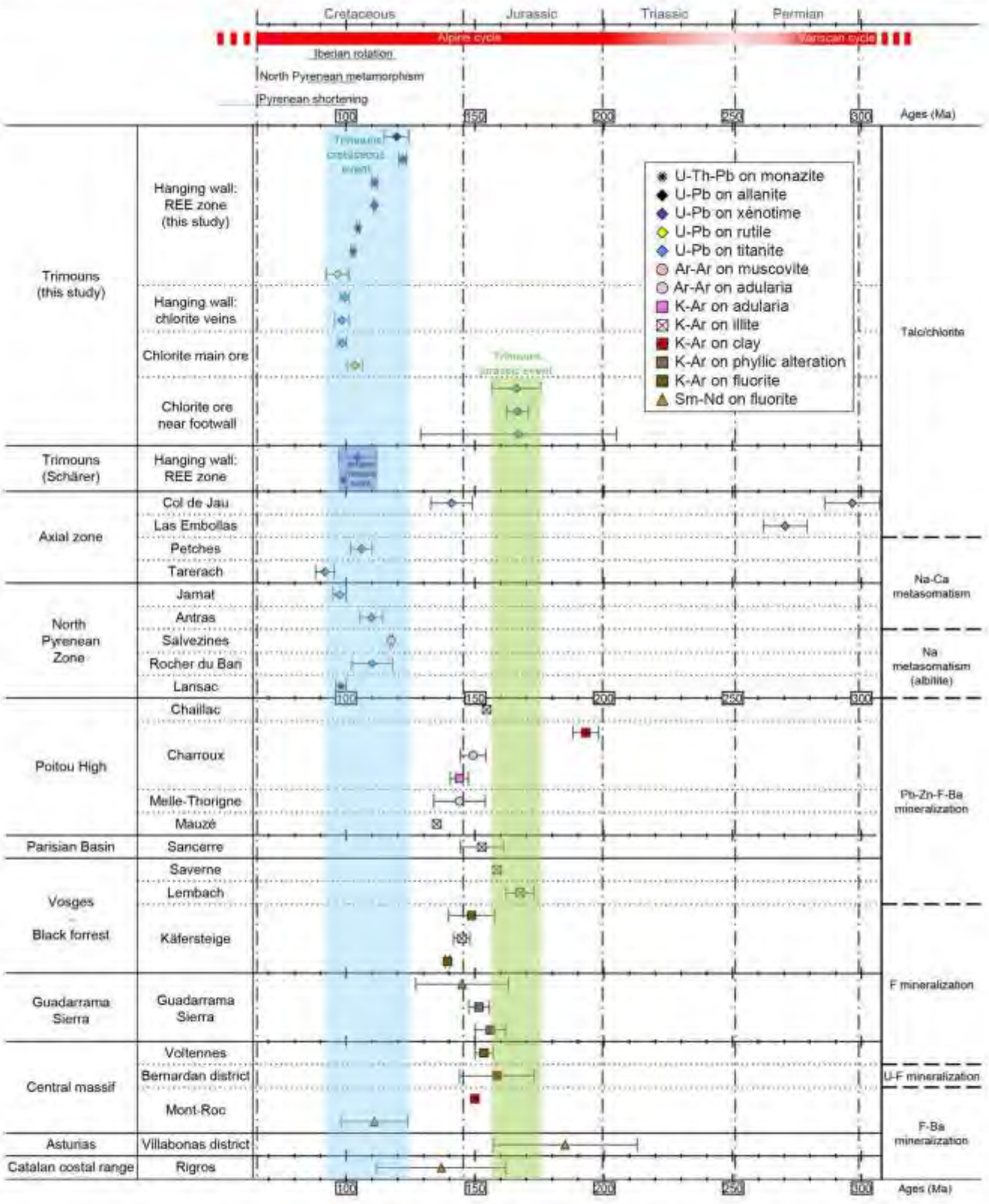

Fig. 6 Timeline for the dating at the Trimouns quarry and in the mineralization in Western Europe

Superposition of the two mineralization events

The ages we have obtained in the Trimouns deposit show the polyphased nature of the mineralization processes. One consequence is that the older mineralizing phases were able to provide a chemical and mechanical control on the youngest phases. In fact, the formation of a chlorite ore at ca. 165 Ma could have introduced a zone of higher permeability and a mechanical weakness along which further deformation and fluid flow would have been enhanced during the Cretaceous extensional event.

To summarize, our dataset shows that the Trimouns talc–chlorite ore was formed during at least two successive hydrothermal events: the first one during the middle Jurassic at ca. 165 Ma and the second one during the Cretaceous between the end of the Aptian and the Cenomanian (122–96 Ma). We propose that the first event produced only chlorite, and the second both talc and chlorite.

Robustness of the U–Pb titanite geochronometers during successive hydrothermal events

Our data emphasize the robustness of the U–Pb titanite system toward fluid circulations as both the Jurassic and the Cretaceous events have been recorded by titanite grains found within the same samples. This means that the U–Pb system of the titanite grains that recorded the oldest, Jurassic event has not been disturbed by the Cretaceous one. The closure temperature of titanite is known to be rather high (up to 750 °C, Frost et al. 2000; Spencer et al. 2013). Given the relatively low temperature proposed for the Cretaceous metasomatic event (around 250–300 °C), it can therefore be expected that the titanite U–Pb isotopic system was not affected. This study demonstrates that the U–Pb chronometers in titanite were not affected by medium temperature (i.e., ca. 300 °C) fluids. However, in the case of the Col de Jau titanite grains, where two events (one Permian and one Jurassic) have been recorded, it appears that the Permian titanite has been affected by a slight Pb loss that we can probably link to the late Jurassic event.

It is very unlikely that the zones that recorded the oldest (Jurassic) event were not affected by the fluids associated with the Cretaceous event, especially when considering the large amount of fluids involved during the younger event. Titanite crystallized as a by-product of chloritization: Titanium hosted in biotite was liberated during the transformation into chlorite and then incorporated within the titanite, together with thorium and uranium. As the second event also occurred in the stability field of chlorite, it is highly probable that titanite was also stable during the Cretaceous event, and by consequence, did not react with the second fluids. Thus, the titanite related to the Jurassic event remained chemically and isotopically closed during the second event.

Regional overview at the scale of the eastern Pyrenees

If we consider all our dataset together, we can identify five successive metasomatic episodes of chlorite and talc formation in the eastern Pyrenees: lower Permian (ca. 296 Ma, chlorite, Jau), middle Permian (ca. 270 Ma, talc, Las Embollas), middle Jurassic (ca. 165 Ma, chlorite, Trimouns), late Jurassic/early Cretaceous (ca. 141 Ma, chlorite, Jau) and middle Cretaceous (120–97 Ma, talc and chlorite, Trimouns) (Fig. 6a).

Permian metasomatic events

We consider that the titanites embedded in a chlorite matrix from sample Jau00-89 and the titanite–quartz association from sample Jau00-96 recorded a Permian hydrothermal event. The emplacement of the Quérigut granodioritic plutons is dated at ca. 307 Ma (Roberts et al. 2000). The relatively short time span of ca. 10 Ma between the pluton emplacement and the chloritization event suggests that the chloritization could be interpreted as a late hydrothermal phase associated with the Variscan magmatism and/or late orogenic deformation.

The middle Permian age of the Las Embollas talc formation event is not easy to interpret. Only one titanite was dated in our sample, and despite a good textural relationship with talc, a genetic link with talc mineralization cannot be made with certainty because there is no evidence of leaching of the silico-aluminous rocks. This limits the interpretation in terms of a hydrothermal Permian event at a regional scale. However, the Permian is recognized as the transition period between the Variscan and Alpine cycles, with the occurrence of transtensional and extensional deformation (Marotta and Spalla 2007). Moreover, a complex but intensive magmatic activity is recorded in the Pyrenean domain during the whole Permian, with a transition between the late Variscan calc-alkaline and late Permian–Triassic tholeiitic magmatisms (Debon et al. 1995; Lago et al. 2004). This suggests that the Permian is potentially a favorable period for the development of metasomatic events in the Pyrenean domain. This constitutes another example of the association between the talc formation processes and the extensional geodynamic context.

Jurassic metasomatic events

In Trimouns, it is not possible to distinguish between the Jurassic and Cretaceous chlorites using either field criteria or the chemical compositions and consequently to identify a Jurassic tectonic event associated with a hydrothermal event. This is maybe a consequence of the very strong tectonic overprint due to the Alpine middle Cretaceous extensional and late Cretaceous to Cenozoic compressional

Table 3 Detailed list of dated mineralizations on Western Europe and references associated

Localization	Mineralization	Age (Ma)	Dating method	References
Trimouns				
Hanging wall: REE zone	Talc–chlorite	119.6 ± 4.8	U–Pb on allanite	This study
		122 ± 1.4	U–Pb on xenotime	
		111.07 ± 0.96		
		111.02 ± 0.46		
		104.64 ± 0.56	U–Th–Pb on monazite	
		102.64 ± 0.65		
		96.6 ± 4.4	U–Pb on rutile	
Hanging wall: chlorite veins	Talc–chlorite	99.6 ± 1.7	U–Pb on titanite	
		98.3 ± 2.8		
Chlorite main ore	Talc–chlorite	98.5 ± 1.7	U–Pb on titanite	
		103.4 ± 3	U–Pb on rutile	
Chlorite ore near footwall	Talc–chlorite	166.1 ± 9.4	U–Pb on titanite	
		166.5 ± 4.2		
		167 ± 38		
Hanging wall: REE zone	Talc–chlorite	97–112	U–Pb on xenotime	Schärer et al. (1999)
		99	U–Pb on monazite	Schärer et al. (1999)
Asturias				
Col de Jau	Chlorite	296.4 ± 7.4	U–Pb on titanite	This study
		141 ± 8	U–Pb on titanite	This study
Las Embollas	Talc	270.4 ± 5.9	U–Pb on titanite	This study
Petches	Na–Ca metasomatism	105.9 ± 4.2	U–Pb on titanite	Fallourd et al. (2014)
Tarerach		91.8 ± 3.6	U–Pb on titanite	Fallourd et al. (2014)
North Pyrenean zone				
Jarnat	Na–Ca metasomatism	97.5 ± 2.5	U–Pb on titanite	Fallourd et al. (2014)
Antras		109.9 ± 4.4	U–Pb on titanite	Fallourd et al. (2014)
Salvezines	Albitite	117.5 ± 0.5	Ar–Ar on muscovite	Boulvais et al. (2007)
Rocher du Bari		110 ± 8	U–Pb on titanite	Poujol et al. (2010)
Lansac		98 ± 2	U–Th–Pb on monazite	Poujol et al. (2010)
Poitou high				
Chaillac	Pb–Zn–F–Ba	154.5	K–Ar on illite	Cathelineau et al. (2012)
Charroux	Pb–Zn–F–Ba	193 ± 5	K–Ar on clay	Cathelineau et al. (2004)
		144.4–154.3	Ar–Ar on adularia	Cathelineau et al. (2012)
		140.5–147.5	K–Ar on adularia	Cathelineau et al. (2012)
Melle-Thorigne	Pb–Zn–F–Ba	144 ± 10	Ar–Ar on adularia	Cathelineau et al. (2012)
Mauzé	Pb–Zn–F–Ba	135.2	K–Ar on illite	Cathelineau et al. (2012)
Parisian Basin				
Sancerre	Pb–Zn–F–Ba	144.4–161.1	K–Ar on illite	Mossman et al. (1992)
Vosges–Black forest				
Saverne	Pb–Zn–F–Ba	158–159	K–Ar on illite	Clauer et al. (2008)
Lembach	Pb–Zn–F–Ba	162–173	K–Ar on illite	Clauer et al. (2008)
Käfersteige	F	139.8–157.7	K–Ar on fluorite	Brockamp and Clauer (2005)
		143.3–146.5	K–Ar on illite	Meyer et al. (2000)
		138.5–140.3	K–Ar on fluorite	Meyer et al. (2000)
Guadarrama sierra				
Guadarrama Sierra	F	145 ± 18	Sm–Nd on fluorite	Galindo et al. (1994)
		151.6 ± 4	K–Ar on phyllic alteration	Caballero et al. (1992)
		156 ± 6	K–Ar on phyllic alteration	Caballero et al. (1992)

Table 3 continued

Localization	Mineralization	Age (Ma)	Dating method	References
French Massif Central				
Voltennes	F	150–157	K–Ar on fluorite	Baudron et al. (1980)
Bernardan district	U–F	158,5 ± 14.5	K–Ar on clays	Patrier et al. (1997)
Mont-Roc	F–Ba	150	K–Ar on clays	Bonhomme et al. (1987)
		111 ± 13	Sm–Nd on fluorite	Muñoz et al. (2005)
Asturias				
Villabonas district	F–Ba	185 ± 28	Sm–Nd on fluorite	Sánchez et al. (2010)
Catalan costal range				
Rigros	F–Ba	137 ± 25	Sm–Nd on fluorite	Piqué et al. (2008)

events, which prevent the identification of Jurassic and/or lower Cretaceous geological structures. In the Pyrenean domain, the Jurassic is classically considered as a quiet tectonic period with only weak and distributed rifting events and small vertical movements at the transition with the Cretaceous (Ziegler and Dèzes 2006; Canérot 2008). The "quiet" Jurassic is, nonetheless, a major period for hydrothermal events as described by Cathelineau et al. (2012) at the scale of Western Europe. These mineralizing events and the Trimouns ore deposit share three common features. All these deposits are linked to (1) brine migration (see Boiron et al. 2005 for Trimouns and Cathelineau et al. 2012 for others), (2) extensive tectonic regimes, and they are (3) spatially distributed around the Pyrenean rift (on both sides and within the Pyrenean domain—Fig. 6b). All these common features strongly suggest that the Jurassic chloritization described in Trimouns fits well with the "major Jurassic fluid event" described by Cathelineau et al. (2012).

The Col de Jau Mesozoic event lies somewhere in between the Jurassic and Cretaceous periods (141 ± 7.8). Titanite dated from sample Jau00-87 is all found in the biotite/chlorite assemblage that probably formed during this hydrothermal event. Even if the titanite grains from sample Jau00-96 are hosted in the quartz, and taking into consideration the robustness of the U–Pb titanite geochronometers during the successive hydrothermal events described above, we consider that the titanite that gives a Jurassic age belongs to a different generation than the titanite formed during the lower Permian. We suggest linking the Col de Jau Mesozoic event to the "major Jurassic fluid event" because it can be compared with the youngest events described by Cathelineau et al. (2012) (Fig. 6a; Table 3).

Cretaceous metasomatic events

Our data unequivocally show that the talc and chlorite formation in Trimouns results from a single—continuous or discontinuous—metasomatic episode which lasted ca. 25–30 Ma between the middle Aptian up to the end of the Cenomanian. This period coincides with the sodic and calco-sodic metasomatism (albitite formation) (Fig. 6a) that affected the pre-Mesozoic basement in both the north Pyrenean massifs and in the northern part of the Axial Zone of the central and eastern Pyrenees (Boulvais et al. 2007; Poujol et al. 2010; Fallourd et al. 2014) (Fig. 1a). The Cretaceous is consequently a key period for metasomatic activity in the Pyrenees. These low to medium temperature (250–350 °C) metasomatisms in the basement began before the high temperature metamorphism (500–600 °C) and the associated magmatism that affected the Mesozoic cover and which both began around 105–108 Ma (Montigny et al. 1986; Golberg and Leyreloup 1990). Moreover, as no high temperature event affected the basement during this period, this strongly suggests a structural decoupling between the basement and the Mesozoic cover at this time: The high temperature event began afterward and developed alongside Trimouns. This is in good agreement with recent data and models regarding the mid-Cretaceous geodynamic setting of the northern side of the Pyrenees, where authors describe extreme thinning of the crust, breakoff of the crust and mantle uprising along a major detachment fault (Lagabrielle and Bodinier 2008; Jammes et al. 2009; Lagabrielle et al. 2010; Clerc et al. 2012). This confirms the association between the extensional context and the talc and chlorite formation processes. The Cretaceous metasomatism in Trimouns could then be considered as one of the first geological records of the crustal extension related to the oblique rifting due to the opening of the Bay of Biscay and the associated rotation of the Iberian plate.

Conclusion

Our dataset shows that the Trimouns talc–chlorite deposit was formed during at least two successive hydrothermal events. The first one that formed chlorite, and which

is dated around 165 Ma (middle Jurassic), was probably related to the major Jurassic hydrothermal event described by Cathelineau et al. (2012) at the scale of Western Europe. The second one formed both talc and chlorite, lasted around 25–30 Ma (122–96 Ma, between the end of the Aptian and the Cenomanian) and constitutes the geological expression of the crustal extension associated with the transtensional rifting event which occurred in the Pyrenean domain in relation to the opening of the Bay of Biscay. The first Jurassic chloritization event constitutes an important precursor, as the formation of a chlorite ore at 165 Ma introduced a zone of higher permeability and mechanical weakness along which further deformation and fluid flow were likely localized during the Cretaceous extensional event.

Our data show a complex succession of hydrothermal events at the scale of the eastern Pyrenees: (1) A late Variscan chloritization event related to hydrothermal circulation probably related to the late Variscan magmatism and deformation; (2) a middle Permian talc formation event, possibly related to extension during the transitional period which separates the Variscan and Alpine cycles; (3) a middle–late Jurassic chlorite formation event, associated with the distributed rifting events described in Western Europe; (4) a Cretaceous talc and chlorite formation event, which could be the result of a pulse-driven activity (three pulses); this last event is spatially and temporally associated with Na–Ca metasomatism in the basement and related to the pre-orogenic hyper-extensional event described in the Pyrenees. The relationship between the formation of large talc and chlorite ores and the extensional tectonic setting is then exemplified by our study.

Our data confirm that the low to medium temperature (250–350 °C) metasomatism (talc, chlorite, albitite) in the basement began before the north Pyrenean high temperature metamorphism (500–600 °C) and the associated magmatism which affected the Mesozoic cover. As no high temperature event affected the basement during this period, this strongly suggests a structural decoupling between the basement and the Mesozoic cover at this time and confirms the breakoff of the crust and mantle uprising along a major detachment fault. The Cretaceous metasomatism in Trimouns could then be considered as one of the first geological records of the crustal extension related to the oblique rifting due to the opening of the Bay of Biscay.

From a more methodological point of view, our study confirms the robustness of titanite to date fluid circulation. Permian and Jurassic titanite grains, which experienced two hydrothermal events, remained closed isotopically. This demonstrates that the U–Pb chronometers of titanite were not affected by medium temperature (i.e., ca. 300 °C) fluids.

Acknowledgments This study was financed by the "Association Nationale de la Recherche et de la Technologie" (ANRT), through a collaborative project between Imerys talc and the GET laboratory, the CNRS, and the University of Toulouse, and by the "Agence Nationale de la Recherche" (ANR) PYRAMID project. We would like to thank everyone who helped with facilitated the preparation of the samples, especially the technical staff of the GET laboratory (Jean François Ménа, Ludovic Menjot and Fabienne de Parseval). We thank Frederic Bec and Guy Bernadi for their experience and mineralogical skills and Sara Mullin for improving the English content. Last but not least, Massimo Tiepolo and an anonymous reviewer are thanked for their constructive comments and Ingo Braun for his editorial handling of this manuscript.

References

Albarède F, Michard-Vitrac A (1978) Age and significance of the North Pyrenean metamorphism. Earth Planet Sci Lett 40:327–332. doi:10.1016/0012-821X(78)90157-7

Aranitis S (1967) Les gisements de talc pyrénéens, Description. Essais d'interprétation de leur genèse. Thèse de Doctorat. BRGM, France

Arthaud F, Matte P (1975) Les décrochements tardi-hercyniens du sud-ouest de l'Europe. Géométrie et essai de reconstitution des conditions de la déformation. Tectonophysics 25:139–171. doi:10.1016/0040-1951(75)90014-1

Azambre B, Rossy M (1976) Le magmatisme alcalin d'age cretacé dans les Pyrenées occidentales et l'arc basque; ses relations avec le metamorphisme et la tectonique. Bull Soc Géol Fr 18:1725–1728. doi:10.2113/gssgfbull.S7-XVIII.6.1725

Barnolas A, Chiron J-C (1995) Synthèse géologique et géophysique des Pyrénées Tome 1 Cycle Hercynien. BRGM, ITGE, Orléans, Madrid

Baudron JC, Jébrak M, Joannes C, Lhegu J, Touray JC, Ziserman A (1980) Nouvelles datations K/Ar sur des filons à quartz et fluorine du Massif Central français. C R Acad Sci Paris 280:951–953

Béziat D, Joron JL, Monchoux P, Treuil M, Walgenwitz F (1991) Geodynamic implications of geochemical data for the Pyrenean ophites (Spain–France). Chem Geol 89:243–262. doi:10.1016/0009-2541(91)90019-N

Boiron M-C, Boulvais P, Cathelineau M, Banks D, Calvayrac N, Hubert G (2005) Fluid circulation at the origin of the Trimouns talc deposit (Pyrenees, France). ECROFI XVIII, Siena

Bonhomme MG, Baubron J-C, Jebrak M (1987) Minéralogie, géochimie, terres rares et âge K-Ar des argiles associées aux minéralisations filoniennes. Chem Geol Isot Geosci Sect 65:321–339. doi:10.1016/0168-9622(87)90012-1

Boulvais P, de Parseval P, D'Hulst A, Paris P (2006) Carbonate alteration associated with talc-chlorite mineralization in the eastern Pyrenees, with emphasis on the St. Barthelemy Massif. Mineral Petrol 88:499–526. doi:10.1007/s00710-006-0124-x

Boulvais P, Ruffet G, Cornichet J, Mermet M (2007) Cretaceous albitization and dequartzification of Hercynian peraluminous granite in the Salvezines Massif (French Pyrénées). Lithos 93:89–106. doi:10.1016/j.lithos.2006.05.001

Brockamp O, Clauer N (2005) A km-scale illite alteration zone in sedimentary wall rocks adjacent to a hydrothermal fluorite vein deposit. Clay Miner 40:245–260. doi:10.1180/0009855054020170

Bronner A, Sauter D, Manatschal G, Péron-Pinvidic G, Munschy M (2011) Magmatic breakup as an explanation for magnetic anomalies at magma-poor rifted margins. Nat Geosci 4:549–553. doi:10.1038/ngeo1201

Bronner A, Sauter D, Manatschal G, Péron-Pinvidic G, Munschy M (2012) Reply to "Problematic plate reconstruction". Nat Geosci 5:677–677. doi:10.1038/ngeo1597

Caballero JM, Casquet C, Galindo C, Gonzalez-Casado JM, Sneilling N, Tornos F (1992) Dating hydrothermal events in the Sierra del Guadarrama, Iberian Hercynian Belt, Spain. Geogaceta 11:18–22

Canérot J (2008) Les Pyrénées: histoire géologique et itinéraires de découverte. Atlantica & BRGM éd, Biarritz

Cathelineau M, Fourcade S, Clauer N, Buschaert S, Rousset D, Boiron M-C, Meunier A, Lavastre V, Javoy M (2004) Dating multistage paleofluid percolations: a K–Ar and 18O/16O study of fracture illites from altered Hercynian plutonites at the basement/cover interface (Poitou High, France). Geochim Cosmochim Acta 68:2529–2542. doi:10.1016/j.gca.2003.10.037

Cathelineau M, Boiron M-C, Fourcade S, Ruffet G, Clauer N, Belcourt O, Coulibaly Y, Banks DA, Guillocheau F (2012) A major Late Jurassic fluid event at the basin/basement unconformity in western France: 40Ar/39Ar and K-Ar dating, fluid chemistry, and related geodynamic context. Chem Geol 322–323:99–120. doi:10.1016/j.chemgeo.2012.06.008

Chevrot S, Villaseñor A, Sylvander M, Benahmed S, Beucler E, Cougoulat G, Delmas P, de Saint Blanquat M, Diaz J, Grimaud F, Lagabrielle Y, Manatschal G, Mocquet A, Pauchet H, Paul A, Péquegnat C, Quillard O, Roussel S, Ruiz M, Wolyniec D (2014) High-resolution imaging of the Pyrenees and Massif Central from the data of the PYROPE and IBERARRAY portable array deployments. J Geophys Res Solid Earth 119:6399–6420. doi:10.1002/2014JB010953

Choukroune P (1976) Structure et évolution tectonique de la zone Nord-Pyrénéenne. Analyse de la déformation dans une portion de chaîne à schistosité subverticale. Société Géologique de France, Paris

Choukroune P, ECORS Pyrénées team (1989) The ECORS Pyrenean deep seismic profile reflection data and the overall structure of an orogenic belt. Tectonics 8:23–39

Choukroune P, Mattauer M (1978) Tectonique des plaques et Pyrénées: sur le fonctionnement de la faille transformante Nord-Pyrénéenne; comparaisons avec des modèles actuels. Bull Soc Géol Fr 20:689–700

Choukroune P, Le Pichon X, Seguret M, Sibuet J-C (1973) Bay of Biscay and Pyrenees. Earth Planet Sci Lett 18:109–118

Clauer N, Liewig N, Ledesert B, Zwingmann H (2008) Thermal history of Triassic sandstones from the Vosges Mountains-Rhine Graben rifting area, NE France, based on K–Ar illite dating. Clay Miner 43:363–379. doi:10.1180/claymin.2008.043.3.03

Clerc C, Lagabrielle Y (2014) Thermal control on the modes of crustal thinning leading to mantle exhumation: insights from the Cretaceous Pyrenean hot paleomargins. Tectonics 33:1340–1359. doi:10.1002/2013TC003471

Clerc C, Lagabrielle Y, Neumaier M, Reynaud J-Y, de Blanquat Saint (2012) Exhumation of subcontinental mantle rocks: evidence from ultramafic-bearing clastic deposits nearby the Lherz peridotite body, French Pyrenees. Bull Soc Géol Fr 183:443–459. doi:10.2113/gssgfbull.183.5.443

Darling JR, Storey CD, Engi M (2012) Allanite U–Th–Pb geochronology by laser ablation ICPMS. Chem Geol 292–293:103–115. doi:10.1016/j.chemgeo.2011.11.012

de Parseval P (1992) Étude minéralogique et géochimique du gisement de talc et chlorite de Trimouns. Thèse de Doctorat, Université de Toulouse III

de Parseval P, Fontan F, Agouy T (1997) Composition chimique des minéraux de terres rares de Trimouns (Ariège, France). C R Acad Sci Paris 324:625–630

de Parseval P, Jiang S, Fontan F et al (2004) Geology and ore genesis of the Trimouns talc chlorite ore deposit. Acta Petrol Sin 20:877–886

de Saint Blanquat M (1993) La faille normale ductile du Saint Barthélémy. Evolution hercynienne des massifs nord-pyrénéens considérée du point de vue de leur histoire thermique. Geodin Acta 6:59–77. doi:10.1080/09853111.1993.11105239

de Saint Blanquat M (1989) La faille normale ductile du massif du Saint Barthélémy (age et signification de l'extension crustale dans la Zone Nord Pyrénéenne). Thèse de Doctorat, Université de Montpellier II, France

de Saint Blanquat M, Brunel M, Mattauer M (1986) Les zones de cisaillements du massif Nord Pyrénéen du Saint Barthélémy, témoins probables de l'extension crustale d'âge crétacé. C R Acad Sci Paris 303:1339–1344

de Saint Blanquat M, Lardeaux JM, Brunel M (1990) Petrological arguments for high temperature extentional deformation in the Pyrenean Variscan crust (Saint Barthélémy Massif, Ariège, France). Tectonophysics 177:245–262. doi:10.1016/0040-1951(90)90284-F

Debon F, Enrique P, Autran A (1995) Magmatisme hercynien. In: Barnolas A, Chiron J-C (eds) Synthèse géologique et géophysique des Pyrénées—Tome 1: Cycle Hercynien. BRGM & ITGE, pp 361–499

Debroas EJ (1990) Le flysch noir albo-cénomanien témoin de la structuration albienne à sénonienne de la Zone nord-pyrénéenne en Bigorre (Hautes-Pyrénées, France). Bull Soc Géol Fr 8 VI 2:273–286. doi:10.2113/gssgfbull.VI.2.273

Delaperrière E, de Saint Blanquat M, Brunel M, Lancelot J (1994) Géochronologie U Pb sur les zircons et monazites dans le massif du Saint Barthélémy. Bull Soc Géol Fr 2:101–112

Denèle Y, Paquette J-L, Olivier P, Barbey P (2012) Permian granites in the Pyrenees: the Aya pluton (Basque Country). Permian granites in the Pyrenees. Terra Nova 24:105–113. doi:10.1111/j.1365-3121.2011.01043.x

Denèle Y, Laumonier B, Paquette J-L, Olivier P, Gleizes G, Barbey P (2014) Timing of granite emplacement, crustal flow and gneiss dome formation in the Variscan segment of the Pyrenees. In: Schulmann, K, Martínez Catalán, JR, Lardeaux, JM, Janousek V, Oggiano G (eds) The Variscan orogeny: extent, timescale and the formation of the European crust, vol 405. Geological Society, London, Special Publications, pp 265–287. doi: 10.1144/SP405.5

Fallourd S, Poujol M, Boulvais P, Paquette J-L, de Saint Blanquat M, Rémy P (2014) In situ LA–ICP–MS U–Pb titanite dating of Na–Ca metasomatism in orogenic belts: the North Pyrenean example. Int J Earth Sci Geol Rundsch 103:667–682. doi:10.1007/s00531-013-0978-1

Fortuné J-P (1971) Contribution à l'étude minéralogique et génétique des talcs pyrénéens. Thèse de Doctorat, Université de Toulouse III, France

Fortuné J-P, Gavoille B, Thiébaut J (1980) Le gisement de talc de Trimouns près Luzenac (Ariège). 26ème Conférence Géologique Internationale, Gisement Français, Fascicule E10

Frost BR, Chamberlain KR, Schumacher JC (2000) Sphene (titanite): phase relations and role as a geochronometer. Chem Geol 172:131–148. doi:10.1016/S0009-2541(00)00240-0

Galindo C, Tornos F, Darbyshire DPF, Casquet C (1994) The age and origin of the barite-fluorite (Pb–Zn) veins of the Sierra del Guadarrama (Spanish Central System, Spain): a radiogenic (Nd, Sr) and stable isotope study. Chem Geol 112:351–364. doi:10.1016/0009-2541(94)90034-5

Gasquet D, Bertrand J-M, Paquette J-L, Lehmann J, Ratzov G, Ascenção Guedes R, Tiepolo M, Coullier A-M, Scaillet S, Nomade S (2010) Miocene to Messinian deformation and hydrothermal activity in a pre-Alpine basement massif of the French western Alps: new U–Th–Pb and argon ages from the Lauzière massif. Bull Soc Géol Fr 181:227–241. doi:10.2113/gssgfbull.181.3.227

Golberg JM, Leyreloup AF (1990) High temperature-low pressure Cretaceous metamorphism related to crustal thinning (Eastern

North Pyrenean Zone, France). Contrib Miner Petrol 104:194–207. doi:10.1007/BF00306443

Golberg J-M, Maluski H (1988) Données nouvelles et mise au point sur l'âge du métamorphisme pyrénéen. C R Acad Sci Paris 306:429–435.

Gong Z, Langereis CG, Mullender TAT (2008) The rotation of Iberia during the Aptian and the opening of the Bay of Biscay. Earth Planet Sci Lett 273:80–93. doi:10.1016/j.epsl.2008.06.016

Gregory CJ, Rubatto D, Allen CM, Williams IS, Hermann J, Ireland T (2007) Allanite micro-geochronology: a LA–ICP–MS and SHRIMP U–Th–Pb study. Chem Geol 245:162–182. doi:10.1016/j.chemgeo.2007.07.029

Höffler P, Vinandy G (2000) Talc de Luzenac: trimouns, un engagement environnemental. Chronique de la recherche minière 541:47–55

Jackson SE, Pearson NJ, Griffin WL, Belousova EA (2004) The application of laser ablation-inductively coupled plasma-mass spectrometry to in situ U–Pb zircon geochronology. Chem Geol 211:47–69. doi:10.1016/j.chemgeo.2004.06.017

Jammes S, Manatschal G, Lavier L, Masini E (2009) Tectonosedimentary evolution related to extreme crustal thinning ahead of a propagating ocean: example of the western Pyrenees: extreme crustal thinning in the Pyrenees. Tectonics. doi:10.1029/2008TC002406

Klötzli E, Klötzli U, Kosler J (2007) A possible laser ablation xenotime U–Pb age standard: reproducibility and accuracy. Geochim Cosmochim Acta 71:A495. doi:10.1016/j.gca.2007.06.019

Lagabrielle Y, Bodinier J-L (2008) Submarine reworking of exhumed subcontinental mantle rocks: field evidence from the Lherz peridotites, French Pyrenees. Terra Nova 20:11–21. doi:10.1111/j.1365-3121.2007.00781.x

Lagabrielle Y, Labaume P, de Saint Blanquat M (2010) Mantle exhumation, crustal denudation, and gravity tectonics during Cretaceous rifting in the Pyrenean realm (SW Europe): Insights from the geological setting of the lherzolite bodies. Tectonics. doi:10.1029/2009TC002588

Lago M, Arranz E, Pocovi A, Galé C, Gil-Imaz A (2004) Permian magmatism and basin dynamics in the southern Pyrenees: a record of the transition from late Variscan transtension to early Alpine extension. Geol Soc Lond Special Publications 223:439–464. doi:10.1144/GSL.SP.2004.223.01.19

Le Pichon X, Bonnin J, Sibuet J-C (1970) La faille nord-pyrénéenne: faille transformante liée à l'ouverture du golfe de Gascogne. C R Hebd Seances Acad Sci Ser D 271:1941–1944

Ludwig KR (1998) On the treatment of concordant uranium-lead ages. Geochim Cosmochim Acta 62:665–676. doi:10.1016/S0016-7037(98)00059-3

Marotta AM, Spalla MI (2007) Permian-Triassic high thermal regime in the Alps: result of late Variscan collapse or continental rifting? Validation by numerical modeling. Tectonics 26:TC4016. doi:10.1029/2006TC002047

Masini E, Manatschal G, Tugend J, Mohn G, Flament J-M (2014) The tectono-sedimentary evolution of a hyper-extended rift basin: the example of the Arzacq-Mauléon rift system (Western Pyrenees, SW France). Int J Earth Sci Geol Rundsch 103:1569–1596. doi:10.1007/s00531-014-1023-8

Meyer M, Brockamp O, Clauer N, Renk A, Zuther M (2000) Further evidence for a Jurassic mineralizing event in central Europe: K–Ar dating of hydrothermal alteration and fluid inclusion systematics in wall rocks of the Käfersteige fluorite vein deposit in the northern Black Forest, Germany. Miner Deposita 35:754–761. doi:10.1007/s001260050277

Moine B, Gavoille B, Thiébaut J (1982a) Géochimie des transformations métasomatiques à l'origine du gisement de talc et chlorite de Trimouns—I. Mobilité des éléments et zonalités. Bull Minéral 105:62–75

Moine B, Gavoille B, Thiébaut J (1982b) Géochimie des transformations métasomatiques à l'origine du gisement de talc et chlorite de Trimouns—II. Approche des conditions physico-chimiques de la métasomatose. Bull Minéral 105:76–88

Moine B, Fortuné J-P, Moreau P, Viguier F (1989) Comparative mineralogy, geochemistry and conditions of formation of two metasomatic talc and chlorite deposits: trimouns (Pyrenees, France) and Rabenwald (Eastern Alps, Austria). Econ Geol 84:1398–1416. doi:10.2113/gsecongeo.84.5.1398

Monchoux P, Fontan F, de Parseval P, Martin RF, Wang RC (2006) Igneous albitite dikes in orogenic lherzolites, western Pyrénées, France: a possible source for corundum and alkali feldspar xenocrysts in basaltic terranes. I. Mineralogical Associations. Can Mineral 44:817–842. doi:10.2113/gscanmin.44.4.817

Montigny R, Azambre B, Rossy M, Thuizat R (1986) K–Ar study of cretaceous magmatism and metamorphism in the Pyrénées: age and length of rotation of the Iberian peninsula. Tectonophysics 129:257–273

Mossman JR, Clauer N, Liewig N (1992) Dating thermal anomalies in sedimentary basins: the diagenetic history of clays minerals in the Triassic sandstones of the Paris basin, France. Clay Miner 27:211–226. doi:10.1180/claymin.1992.027.2.06

Muñoz JA (1992) Evolution of a continental collision belt: ECORS-Pyrenees crustal balanced cross-section. In: McClay KR (ed) Thrust tectonics. Chapman and Hall, London, pp 235–246

Muñoz M, Premo WR, Courjault-Radé P (2005) Sm–Nd dating of fluorite from the worldclass Montroc fluorite deposit, southern Massif Central, France. Miner Depos 39:970–975. doi:10.1007/s00126-004-0453-9

Olivet J-L (1996) La cinématique de la plaque ibérique. Bull Cent Rech Explor Prod Elf Aquitaine 20:131–195

Paquette J-L, Tiepolo M (2007) High resolution (5 μm) U–Th–Pb isotope dating of monazite with excimer laser ablation (ELA)-ICPMS. Chem Geol 240:222–237. doi:10.1016/j.chemgeo.2007.02.014

Paquette J-L, Piro J-L, Devidal J-L, Bosse V, Didier A (2014) Sensitivity enhancement in LA–ICP–MS by N2 addition to carrier gas: application to radiometric dating of U–Th–bearing minerals. Agil ICP–MS J 58:4–5

Passchier CW (1982) Pseudotachylyte and the development of ultramylonite bands in the Saint Barthélemy Massif. J Struct Geol 4:69–79. doi:10.1016/0191-8141(82)90008-6

Patrier P, Beaufort D, Bril H, Bonhomme M, Fouillac AM, Aumatre R (1997) Alteration-mineralization at the Bernardan U deposit (Western Marche, France): the contribution of alteration petrology and crystal chemistry of secondary phases to a new genetic model. Econ Geol 92:448–467. doi:10.2113/gsecongeo.92.4.448

Pedersen RB, Dunning GR, Robins B (1989) U–Pb ages of nepheline syenite pegmatites from the Seiland Magmatic Province, N Norway. In: Gayer RA (ed) The Caledonide geology of Scandinavia. Graham and Trotman, London, pp 3–8

Pin C, Vielzeuf D (1983) Granulites and related rocks in Variscan median Europe: a dualistic interpretation. Tectonophysics 93:47–74

Pin C, Paquette JL, Monchoux P, Hammouda T (2001) First field-scale occurrence of Si–Al–Na–rich low-degree partial melts from the upper mantle. Geology 29:451–454. doi:10.1130/0091-7613(2001)029<0451:FFSOOS>2.0.CO;2

Pin C, Monchoux P, Paquette J-L, Azambre B, Wang RC, Martin RF (2006) Igneous albitite dikes in orogenic lherzolites, western Pyrénées, France: a possible source for corundum and alkali feldspar xenocrysts in basaltic terranes. II. Geochemical and petrogenetic considerations. Can Mineral 44:843–856. doi:10.2113/gscanmin.44.4.843

Piqué À, Canals À, Grandia F, Banks DA (2008) Mesozoic fluorite veins in NE Spain record regional base metal-rich brine circulation through basin and basement during extensional events. Chem Geol 257:139–152. doi:10.1016/j.chemgeo.2008.08.028

Poujol M, Boulvais P, Kosler J (2010) Regional-scale Cretaceous albitization in the Pyrenees: evidence from in situ U–Th–Pb dating of monazite, titanite and zircon. J Geol Soc 167:751–767. doi:10.1144/0016-76492009-144

Raguin E (1958) Conceptions sur la genèse du talc de Corneilla. Réunion extraordinaire dans les Pyrénées Orientales. Bull Soc Géol Fr 6:925

Roberts MP, Pin C, Clemens JD, Paquette J-L (2000) Petrogenesis of mafic to felsic plutonic rock associations: the calc-alkaline Quérigut complex, French Pyrenees. J Petrol 41:809–844. doi:10.1093/petrology/41.6.809

Sánchez V, Cardellach E, Corbella M et al (2010) Variability in fluid sources in the fluorite deposits from Asturias (N Spain): Further evidences from REE, radiogenic (Sr, Sm, Nd) and stable (S, C, O) isotope data. Ore Geol Rev 37:87–100. doi:10.1016/j.oregeorev.2009.12.001

Schärer U, de Parseval P, Polvé M, de Saint Blanquat M (1999) Formation of the Trimouns talc chlorite deposit from persistent hydrothermal activity between 112 and 97 Ma. Terra Nova 11:30–37. doi:10.1046/j.1365-3121.1999.00224.x

Séguret M (1972) Etude tectonique des nappes et séries décollées de la partie centrale du versant sud des Pyrénées: caractère synsédimentaire, rôle de la compression et de la gravité. Thèse de Doctorat. Université de Montpellier II, France

Sibuet J-C, Srivastava SP, Spakman W (2004) Pyrenean orogeny and plate kinematics. J Geophys Res. doi:10.1029/2003JB002514

Spencer KJ, Hacker BR, Kylander-Clark ARC, Andersen TB, Cottle JM, Stearns MA, Poletti JE, Seward GCE (2013) Campaign-style titanite U–Pb dating by laser-ablation ICP: implications for crustal flow, phase transformations and titanite closure. Chem Geol 341:84–101. doi:10.1016/j.chemgeo.2012.11.012

Stacey JS, Kramers JD (1975) Approximation of terrestrial lead isotope evolution by a two-stage model. Earth Planet Sci Lett 26:207–221. doi:10.1016/0012-821X(75)90088-6

Storey CD, Jeffries TE, Smith M (2006) Common lead-corrected laser ablation ICP–MS U–Pb systematics and geochronology of titanite. Chem Geol 227:37–52. doi:10.1016/j.chemgeo.2005.09.003

Sun J, Yang J, Wu F, Xie L, Yang Y, Liu Z, Li X (2012) In situ U-Pb dating of titanite by LA-ICPMS. Chinese Science Bulletin 57:2506–2516. doi:10.1007/s11434-012-5177-0

Tucholke BE, Sibuet J-C (2012) Problematic plate reconstruction. Nat Geosci 5:676–677. doi:10.1038/ngeo1596

Van Achterbergh E, Ryan CG, Jackson SE, Griffin WL (2001) Data reduction software for LA–ICP–MS: appendix. In: Sylvester PJ (ed) Laser ablation-ICP-mass spectrometry in the earth sciences: principles and applications. Mineralogical Association of Canada, Ottawa, pp 239–243

Vidal O, Parra T, Trotet F (2001) A thermodynamic model for Fe-Mg aluminous chlorite using data from phase equilibrium experiments and natural pelitic assemblages in the 100° to 600°C, 1 to 25 kb range. Am J Sci 301:557–592

Vielzeuf D (1984) Relations de phases dans le faciès granulitique et implications géodynamiques. L'exemple des granulites des Pyrénées. Thèse de Doctorat. Université de Clermont II, France

Wiewióra A, Weiss Z (1990) Crystallochemical classifications of phyllosilicates based on the unified system of projection of chemical composition: II. The chlorite group. Clay Miner 25:83–92

Zack T, Stockli DF, Luvizotto GL, Barth MG, Belousova H, Wolfe MR, Hinton RW (2011) In situ U–Pb rutile dating by LA–ICP–MS: 208Pb correction and prospects for geological applications. Contrib Miner Petrol 162:515–530. doi:10.1007/s00410-011-0609-4

Ziegler PA, Dèzes P (2006) Crustal evolution of Western and Central Europe. Geol Soc Lond Mem 32:43–56. doi:10.1144/GSL.MEM.2006.032.01.03

Zwart HJ (1954) La géologie du massif du Saint-Barthélémy, Pyrénées, France. Thèse de Doctorat, Université de Leiden, Pays-Bas

B) Résultats complémentaires

L'étude de Boutin et al. (2015) est axée autour des minéralisations. Cependant les faciès paléozoïques sont associés à de nombreux événements géologiques autres que l'hydrothermalisme mésozoïque.

(1) Description des roches étudiées

Les marbres gris bleuté du toit (Silurien) situés au contact de la minéralisation talco-chloriteuse (**Fig. IV-2**) ont été altérés en surface par les fluides métasomatiques. Ils présentent une altération talco-chloriteuse en bordure de banc exclusivement. La roche (hors bordure altérée) est constituée surtout de calcite mais aussi de biotite, de quartz, d'épidote, de titanite et de minéraux accessoires (**Fig. IV-3**).
Cette composition minérale est proche de celle des cornéenne (un faciès métamorphique de basse pression). La présence de titanite au sein de la matrice carbonatée est particulièrement intéressante grâce à son potentiel de géochronomètre (Frost et al., 2000) ; de par sa température de fermeture estimée au-dessus de 500°C (Gascoyne, 1986), la titanite est un minéral de choix pour dater les métamorphismes de bas grade (Fallourd et al., 2014).

Figure IV-2 : Vue du contact entre les marbres gris bleuté et les talcitites.

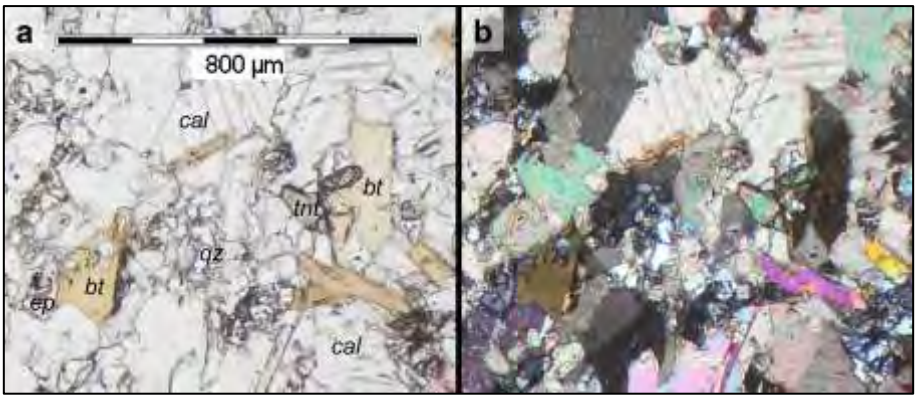

Figure IV-3 : Marbres gris bleuté (échantillon M1S3) observés au microscope optique (x40) en (**a**) ***LSP***, et en (**b**) ***LPA*** ; calcite (cal), biotite (bt), épidote (ep), qz (quartz), tnt (titanite).

(2) Méthode analytique et résultats

Nous avons mené une étude géochronologique sur les titanites de l'échantillon M1S3 avec la méthode à ablation laser couplée à un ICP-MS. Les travaux ont été réalisés à l'Université de Rennes 1 (laboratoire Géosciences Rennes) sous la supervision de Marc Poujol avec un système d'analyse composé d'un spectromètre ICP-MS Agilent 7700, d'un laser Excimer 193 nm ESI (NWR193UC) à durée d'impulsion ultra-courte (<5ns) entièrement piloté par ordinateur, et d'une cellule d'ablation à deux volumes. Le protocole analytique est similaire à celui décrit dans (Boutin et al., 2016) : deux standards ont été utilisés, un zircon « GJ-1 » daté à 602 Ma (Jackson et al., 2004) et une titanite datée à 520 Ma (Pedersen et al., 1989) provenant du Lillebukt Alkaline Complex au nord de la Norvège ; les spots d'analyses ont été faits sur un diamètre de 50 µm. Les données ont été traitées avec le logiciel Glitter (Van Achterbergh et al., 2001). Les âges ont été calculés avec le logiciel isoplot 4.0 (Ludwig, 1998). Les titanites pouvant contenir une part de Pb commun non négligeable, les résultats ont été reportés dans des diagrammes Tera-Wasserburg (rapport $^{207}Pb/^{206}Pb$ et $^{206}Pb/^{238}U$).

Nous avons pu analyser huit minéraux de titanites automorphes (pour 10 spots d'analyses) dans une lame mince. Les résultats (**Fig. IV-4** et **Fig. IV-5**) sont assez discordants et définissent une droite (discordia) dont l'intercept inférieur avec la concordia (diagramme Tera-Wasserburg) est situé à **292,2 ±4,2 Ma** (MSWD = 2.2). L'intercepte supérieur situé à **4490 ±27 Ma** est compatible avec la composition en plomb commun à 290 Ma (rapport 207Pb/206Pb = env. 0.855) suivant le modèle de Stacey et Kramers (1975). Si on force/ancre cette composition, on obtient un âge similaire de **293,4 ±2,1 Ma** (MSWD = 2.1). Nous interprétons donc l'âge de **292,2 ±4,2 Ma** comme celui de la cristallisation des titanites de cet échantillon.

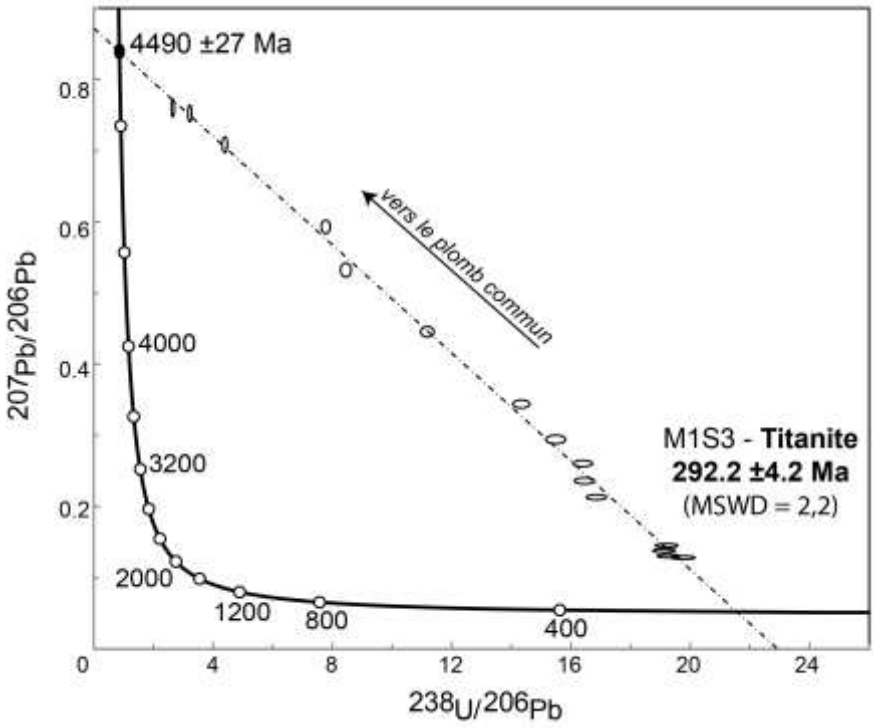

Figure IV-4 : Diagramme concordia Tera-Wasserburg pour les titanites de l'échantillon M1S3.

Grain.spot	Rapports isotopiques					
	$^{207}Pb/^{235}U$	Erreur	$^{206}Pb/^{238}U$	Erreur	$^{207}Pb/^{206}Pb$	Erreur
1.1	39.5472	0.51447	0.37752	0.00503	0.75986	0.00832
2.1	32.22828	0.41108	0.31081	0.00401	0.75215	0.0078
3.1	10.50904	0.13384	0.12857	0.00165	0.59289	0.00614
4.1	0.93296	0.01273	0.05187	0.00068	0.13048	0.00153
4.2	0.89608	0.0127	0.0506	0.00067	0.12846	0.00161
4.3	5.49185	0.07145	0.08941	0.00118	0.44553	0.00491
4.4	0.99497	0.01358	0.05229	0.00069	0.13802	0.00162
5.1	1.04412	0.01402	0.05206	0.00068	0.14549	0.00166
5.2	1.97905	0.02724	0.06078	0.00082	0.2362	0.00289
6.1	8.68371	0.11683	0.11836	0.00165	0.53219	0.00649
7.1	22.23177	0.28442	0.22772	0.00295	0.70816	0.00741
8.1	2.19079	0.02871	0.06098	0.0008	0.26057	0.00287
8.2	1.74462	0.02313	0.05934	0.00078	0.21325	0.00239
9.1	3.30839	0.0428	0.06974	0.00091	0.34411	0.00369
10.1	2.62013	0.0374	0.06457	0.00091	0.29433	0.00394

Figure IV-5 : Données isotopiques uranium-plomb pour les titanites de l'échantillon M1S3 (erreurs à 1σ).

(3) Discussion

Les âges des grains de titanite nous permettent d'estimer l'âge du métamorphisme qui a affecté les marbres gris bleuté. Nous pouvons donc relier cette marmorisation à la période permienne (Cisuralien). Dans le massif du Saint Barthélémy, cette marmorisation fait écho à la migmatisation des roches précambriennes et paléozoïques inférieures (ca. 300 Ma - Delaperriere et al., 1994). Des études récentes montrent que l'épisode thermique tardi-varisque sur le Saint Barthélémy pourrait être subdivisé en deux événements à ca. 300 et ca. 280 Ma (Lemirre, 2015 - communication orale), ce qui situe nos âges à une période charnière entre deux épisodes thermiques. Cependant, l'impact sur les calcaires siluriens d'un ou plusieurs épisodes thermiques chauds et profonds est difficile à estimer car *(1)* le flux de chaleur généré lors la migmatisation n'est pas précisément connu, *(2)* l'épaisseur de roches affectées par ce flux restent méconnue d'autant plus que la série cambro-ordovicienne est extrêmement réduite à Trimouns. On retiendra néanmoins qu'un (ou plusieurs) épisode(s) thermique(s) profond (migmatisation) à la fin du cycle varisque est en accord avec le métamorphisme Haute Température dans les terrains siluriens sus-jacents (voir chapitre III).

(4) Conclusion

Nos résultats montrent un épisode de marmorisation dans la base des séries siluriennes du toit de Trimouns à la période tardi-varisque (ca. 290 Ma). Les évènements hydrothermaux mésozoïques (Schärer et al., 1999 ; Boutin et al., 2016) aux températures moyennes observées à Trimouns (env. 300°C - Parseval, 1992 ; Boiron et al., 2005) n'ont pas affecté les titanites des marbres gris bleuté, attestant de la robustesse de la titanite aux fluides de températures peu élevées.